Title: Myc and Tor drive growth and cell competition in the regeneration blastema of *Drosophila* wing imaginal discs

Running title: Myc and Tor in Regeneration

Felicity Ting-Yu Hsu[1] and Rachel Smith-Bolton[1]

[1] Cell and Developmental Biology, University of Illinois at Urbana-Champaign, Urbana, IL 61801, USA

*Author for correspondence (rsbolton@illinois.edu)

Keywords: Regeneration, Drosophila, Myc, Tor, Cell Competition

Summary statement

Drosophila wing disc regeneration is characterized by concentric growth zones controlled by the Myc transcription factor, the Tor signaling pathway, and Myc-induced cell competition.

Abstract

During the regeneration of injured or lost tissues, the regeneration blastema serves as a hub for robust growth. *Drosophila* imaginal discs are a genetically tractable and simple model system for the study of regeneration and organization of this regrowth. Key signals that contribute to regenerative growth in these discs, such as ROS, Wnt/Wg, JNK, p38, JAK/STAT, and the Hippo pathway, have been identified. However, a detailed exploration of the spatial organization of regrowth, the factors that directly drive this growth, and the consequences of activating drivers of regeneration has not been undertaken. Here, we find that regenerative growth in imaginal discs is controlled by the transcription factor Myc and by Tor signaling, which additively drive proliferation and translation in the regeneration blastema. The spatial organization of growth in the blastema is arranged into concentric growth zones defined by Myc expression, elevated Tor activity, and elevated translation. In addition, the increased Myc expression in the innermost zone induced Xrp1-independent cell competition-like death in the adjacent zones, revealing a delicate balance between driving growth and inducing death in the regenerating tissue.

Introduction

Regeneration is a phenomenon through which some animals restore tissues or organs after damage. This regrowth often occurs through proliferation of a group of undifferentiated and robustly growing cells at the damage site, called a blastema (reviewed in Londono et al., 2018). To study tissue regeneration, we use *Drosophila* wing imaginal discs as a model. The ability of these appendage primordia to regenerate during the larval stage was discovered when the imaginal discs were cut and incubated in the abdomens of female flies (Hadorn and Buck, 1962). Two decades later, blastema-like cells were shown to be robustly proliferating at the wound site in leg and wing imaginal discs (Abbott et al., 1981; O'Brochta and Bryant, 1987). Subsequent searches for signaling pathways important for regenerative growth identified Jun N-terminal Kinase (JNK) signaling as crucial for disc regeneration after fragmentation (Bosch et al., 2005), and lineage tracing demonstrated that cells experiencing JNK signaling were the origin of the regeneration blastema (Bosch et al., 2008). More recently, genetic ablation systems have replaced fragmentation in regeneration studies, where localized massive cell death is generated through overexpression of pro-apoptotic genes (Fox et al., 2020). In these ablation systems, blastema cells were also found around the wound sites during regeneration (Smith-Bolton et al., 2009). To better define the blastema, two research groups (Floc'hlay et al., 2023; Worley et al., 2022) used single-cell RNA-sequencing (scRNA-seq) to characterize blastema cells by gene expression. This approach identified two clusters of cells with expression of signaling molecules such as Wg and Upd3 and transcription factors such as Ets21C that define the blastema (Floc'hlay et al., 2023; Worley et al., 2022). However, gene expression alone may not capture all changes in cell behavior and may not identify all cells contributing to the regenerating tissue.

The ability of imaginal discs to form a blastema is reduced during the late third instar due to an increase in the hormone ecdysone, which silences damage-responsive signals (Halme et al., 2010; Harris et al., 2016; Jaszczak and Halme, 2016). During normal development, low ecdysone levels maintain larval development and growth of the imaginal discs, while a burst of high ecdysone production triggers developmental transitions such as molting or pupariation (Thummel, 2001). Damage during the early-

and mid-third larval instar induces secretion of the relaxin-like peptide *Drosophila* insulin-like peptide 8 (ILP8), which reduces systemic ecdysone and delays the surge to prolong larval development. This reduced ecdysone also reduces imaginal disc growth outside of the damaged area (Colombani et al., 2012; Garelli et al., 2012; Halme et al., 2010; Jaszczak and Halme, 2016; Jaszczak et al., 2015; Jaszczak et al., 2016; Karanja et al., 2022; Katsuyama et al., 2015). Therefore, the regeneration blastema must override the global reduction of growth due to low ecdysone levels.

In this paper, we demonstrate that two factors drive blastema growth additively – the transcription factor Myc and the Target of Rapamycin (Tor) signaling pathway. Both Myc transcription and Tor signaling were upregulated during regeneration. Reducing their expression or kinase activity reduced proliferation and translation in the blastema. Interestingly, the area with activated Tor signaling extended beyond the area with high Myc expression, establishing concentric zones of blastema growth.

Myc expression level differences between adjacent cell populations lead to cell competition or super-competition during normal development (De La Cova et al., 2004; De La Cova et al., 2014; Meyer et al., 2014; Morata, 2021). Cell competition occurs when neighboring cells have different fitness levels, and “loser cells” are eliminated by cell death, while “winner cells” replace the loser cells, and a range of mechanisms have been proposed to carry out the fitness comparison (Reviewed in Morata, 2021). Death of the loser cells can involve autophagy (Nagata et al., 2019) and expression of the transcription factor Xrp1 (Baillon et al., 2018; Blanco et al., 2020; Kiparaki et al., 2022; Lee et al., 2018; Ochi et al., 2021).

Interestingly, proteotoxic stress as assessed by increased levels of phosphorylated eIF2α has been reported in loser cells during cell competition induced by mutations in ribosome genes (Baumgartner et al., 2021), and phosphorylated eIF2α is sufficient to induce loser cell fate (Kiparaki et al., 2022). However, increased phosphorylation of eIF2α also occurs in winner cells during super-competition induced by Myc overexpression, although these

cells are protected from this proteotoxic stress and do not undergo apoptosis (Paul et al., 2024).

Notably, these mechanisms that govern cell competition in wing imaginal discs have predominantly been studied using induced clones of genetically distinct cell populations (Reviewed in Khandekar and Ellis, 2024). While the regeneration blastema has high expression of Myc, it was unclear whether the Myc expression differences that arose during regeneration would lead to competitive behaviors similar to those induced by clones of cells in an undamaged disc and whether the mechanism would align with any of the established models of cell competition.

Here, we show that cell death is increased in the cells adjacent to the high Myc-expressing cells in the blastema. Furthermore, this cell death was suppressed when Myc expression was reduced. The cells adjacent to the high-Myc cells showed an increase in autophagy and eIF2α phosphorylation, similar to loser cells in cell competition. However, we did not find elevated Xrp1 expression, and heterozygosity for Xrp1 did not eliminate Myc-induced cell death in regenerating wing discs. Therefore, the heterogeneity and complex signaling in the regeneration blastema likely leads to a type of cell competition that is not identical to the competition induced when two sets of cells differ by only one factor.

Thus, wing disc regeneration involves not only robust regrowth but also increased cell death, suggesting that there is a dynamic balance between growth and death, providing new insights into the microenvironment of regenerating tissue.

Results

Myc and Tor drive blastema growth

To study regeneration in the *Drosophila* wing imaginal disc, we used a genetic ablation system in which tissue damage can be induced with spatial and temporal precision (Smith-Bolton et al., 2009). This ablation system uses the UAS/Gal4 transcriptional system, where a Gal4 in the *rotund* (*rn*) locus directs the expression of the pro-apoptotic gene *reaper* (*rpr*) in the wing imaginal disc pouch (Fig. 1A). In addition, the Gal4 activity

131 is constrained by Gal80^{ts} at 18°C but not at 30°C. We raised the larvae in an 18°C
132 incubator for seven days after egg-laying, when the larvae reach the early third instar
133 stage, then transferred the larvae to a 30°C water bath for 24 hours to activate apoptosis.
134 After the 24-hour temperature shift, the larvae were returned to 18°C. This time point was
135 considered recovery time 0 (R0) (Fig. 1A).
136
137 To characterize growth in a regenerating wing disc, we examined proliferation in
138 undamaged and regenerating discs 24 hours after the end of tissue damage, or recovery
139 time 24 (R24). We used EdU incorporation to mark cells in S-phase and anti-phospho-
140 histone H3 (PH3) immunostaining to mark cells in mitosis. We compared the undamaged
141 wing pouch, whose outer edge is marked by the inner ring of Wg expression (Fig.
142 S1A,A')(Swarup and Verheyen, 2012), and the regeneration blastema, which is marked
143 by Wg expression throughout (Fig. S1B,B') (Smith-Bolton et al., 2009; Worley et al., 2022).
144 In undamaged wing discs, cells in S-phase were distributed evenly throughout the wing
145 disc (Fig. 1B). However, after tissue damage, the blastema had increased EdU
146 incorporation (Fig. 1C,D), suggesting more cells were in S phase. Similarly, mitotic cells
147 appeared uniform throughout an undamaged wing disc (Fig. 1E), but the regeneration
148 blastema had an increased number of mitotic cells (Fig. 1E,F,G).
149
150 Next, we asked if regeneration also involves increased growth driven by protein
151 translation. To examine protein translation, we used the O-propargyl-puromycin (OPP)
152 assay, which marks newly synthesized protein by incorporating a puromycin analog
153 detected by click chemistry. In undamaged discs, translation seemed evenly distributed
154 throughout (Fig. 1H). However, after tissue damage, the blastema had markedly
155 increased translation (Fig. 1I,J).
156
157 Given that proliferation and translation were elevated in the regeneration blastema, we
158 asked what drives this robust growth. To answer this question, we examined Ecdysone
159 Receptor (EcR) activity, glycolysis, Myc expression, and Tor signaling. We first asked
160 whether blastema cells escape reduced growth caused by reduced ecdysone by
161 upregulating activity of the EcR (Fig. S1). Indeed, our transcriptional profile of the

regeneration blastema showed slight upregulation of *EcR*, a log2 increase of 1.16 (p=0.00005)(Khan et al., 2017). In addition, EcR activity is increased during later regeneration (R32) and is important for regeneration (Terry et al., 2024). To assess EcR activity at R24 we used the *7xEcRE-GFP* reporter, which has seven EcR response elements (EcREs) upstream of GFP (Hackney et al., 2007; Terry et al., 2024). In undamaged wing discs, the EcRE-GFP reporter was active in the entire wing pouch (Fig. S1C), and was not elevated in the blastema at R24 (Fig. S1D), indicating that enhanced EcR activity does not drive growth at R24.

Recent work on zebra fish fin regeneration demonstrated that glycolysis is increased during early regeneration due to the upregulation of lactate dehydrogenase (Ldh) (Brandão et al., 2022). Therefore, we asked whether increased glycolysis and lactate dehydrogenase might be driving the growth in the regeneration blastema. We used a reporter line for *Lactate dehydrogenase* (*Ldh*) expression, *Ldh-GFP*^{Genomic} (Bawa et al., 2020; Rai et al., 2024), which did not show increased expression in the blastema (Fig. S1E,F). Thus, upregulated Ldh does not drive the robust growth in the regeneration blastema.

Myc is a transcription factor that regulates cell growth by promoting proliferation and translation (Bellosta and Gallant, 2010; Grewal et al., 2005; Johnston et al., 1999) and is important for regeneration in multiple animals, including Hydra, Axolotl, *Xenopus*, and zebrafish (as reviewed in Ascanelli et al., 2024). In *Drosophila* imaginal discs, Myc is highly expressed in the blastema, overexpression of Myc leads to better regeneration, and reduction of Myc causes poor regeneration (Abidi et al., 2023; Harris et al., 2020; Serras and Bellosta, 2024; Smith-Bolton et al., 2009). To determine whether Myc is upregulated through transcription, we used a *Myc-lacZ* reporter line. In undamaged discs, *Myc-lacZ* expression was observed throughout the pouch, with a slight reduction at the dorsal-ventral boundary (Fig. 1K). At R24, *Myc-lacZ* was upregulated in the regeneration blastema (Fig. 1L-M). We previously found that Myc expression was difficult to reduce during regeneration, either through RNAi knockdown or use of a heterozygous mutation (Abidi et al., 2023), suggesting that its expression is tightly regulated.

193

194 Tor regulates translation by phosphorylating ribosomal p70 S6 kinase I (S6K), which in
195 turn phosphorylates ribosomal protein S6 (RpS6) (reviewed in Frappaolo and Giansanti,
196 2023). We examined Tor pathway activity through anti-phospho-RpS6 (p-S6)
197 immunostaining (Romero-Pozuelo et al., 2017). In an undamaged wing disc, elevated p-
198 S6 occurred in a patchy pattern (Fig. 1N), consistent with previous studies (Romero-
199 Pozuelo et al., 2017). At R24, p-S6 was enhanced in the regenerating blastema (Fig. 1O-
200 P), suggesting that the Tor pathway might also be an important driver of growth during
201 wing disc regeneration.

202

203 **Myc promotes regenerative growth in a damaged wing disc**

204 To determine the extent to which Myc contributes to the growth of the blastema, we
205 examined proliferation and protein synthesis in regenerating wing discs with reduced Myc
206 expression. We have previously shown that animals hemizygous for the hypomorphic
207 allele Myc^{P0} had reduced Myc levels in regenerating wing discs and regenerated poorly
208 (Abidi et al., 2023)(Fig. S2A,B). By comparing EdU incorporation in the control and the
209 Myc^{P0} regeneration blastemas (Fig. 2A-B), we found a reduction in EdU when Myc levels
210 were reduced (Fig. 2C). Similarly, measurement of mitoses by anti-PH3 staining showed
211 fewer mitotic cells in the Myc^{P0} blastema (Fig. 2D-F). We used the OPP assay to measure
212 protein translation and found that Myc^{P0} regenerating discs had reduced translation (Fig.
213 2G-I). Thus, Myc promotes growth in the regeneration blastema by promoting translation
214 as well as proliferation.

215

216 As Myc regulates growth and translation at least partially through ribosomal biogenesis
217 (Grewal et al., 2005), we examined ribosomal biogenesis by measuring the size of the
218 nucleoli using an anti-Fibrillarin antibody. We measured 10 nucleoli in a 200-pixel^2 area
219 in the hinge and pouch or blastema of each disc. In undamaged discs, the pouch nucleoli
220 and the hinge nucleoli were similar in size (Fig. 2J-L,V). In regenerating wing discs, the
221 blastema cells had larger nucleoli than the hinge cells (Fig. 2M-O,V). Importantly, the
222 nucleoli in the blastema cells were also larger than those in undamaged discs (Fig.
223 2K,N,V).

224

225 To determine whether the larger nucleoli in the blastema were due to increased Myc
226 expression, we measured nucleoli in undamaged and damaged *Myc*^{P0} discs. In *Myc*^{P0}
227 undamaged discs, the nucleoli were the same size in the wing pouch and in the hinge
228 (Fig. 2P-R,V) and smaller than those in control undamaged discs (Fig. 2V). This result
229 was expected because Myc expression was reduced throughout the disc. In *Myc*^{P0}
230 regenerating discs, nucleoli in the *Myc*^{P0} blastema were still larger than the nucleoli in the
231 *Myc*^{P0} hinge (Fig. 2S-U,V) but were smaller than those in the control blastema (Fig.
232 2N,T,V). Therefore, Myc contributes to the growth of the regeneration blastema but does
233 not account for all of the increase in ribosomal production and nucleolus size.

234

235 **Tor promotes growth in the regeneration blastema**

236 To determine the extent to which Tor signaling contributes to regeneration, we reduced
237 Tor activity using animals heterozygous for *Tor*^{2L1}, a hypomorphic allele that has impaired
238 kinase activity due to a single amino acid change in the kinase domain (Oldham et al.,
239 2000). To confirm that Tor activity was reduced in *Tor*^{2L1}/+ regenerating discs, we
240 assessed anti-p-S6 immunostaining at R24 (Fig. 3A-B), using Wg as a blastema marker
241 (Fig. S3A-B). As expected, p-S6 signal was reduced in the blastemas of *Tor*^{2L1}/+ discs
242 (Figs. 3A-C, S3A-B). In addition, we examined the adult wings that developed from
243 regenerated discs of *Tor*^{2L1}/+ flies as a proxy for how well regeneration occurred in the
244 imaginal disc. The *Tor*^{2L1}/+ flies had smaller wings after disc regeneration, indicating that
245 the imaginal discs had regenerated poorly (Fig. S3C).

246

247 We assessed proliferation in *Tor*^{2L1}/+ regenerating discs using EdU incorporation and
248 anti-PH3 staining (Figs. 3D-I, S3D-E). EdU intensity was reduced when Tor activity was
249 reduced (Fig. 3D-F). Similarly, PH3 counts per area showed that the number of mitotic
250 cells was reduced when Tor activity was reduced (Figs. 3G-I, S3D-E).

251

252 We examined protein translation using the OPP assay, and we found reduced protein
253 translation in the blastema when Tor signaling was reduced (Figs. 3J-L, S3F-G). Thus,
254 we concluded that Tor signaling promotes regeneration blastema growth by regulating

255 both proliferation and translation. Interestingly, we noticed that the blastema area, marked
256 by Wg expression, was smaller than the area with upregulated translation (Fig. 3J-K),
257 suggesting that regenerative growth may be elevated outside of the zone marked by
258 expression of blastema genes.
259
260 Next, we asked if Tor enhances growth in part by enhancing ribosomal biogenesis.
261 However, the nucleoli in the blastemas of *Tor*^{2L1}/+ discs were not smaller than those in
262 the controls (Fig. S3H-N). We wondered if the heterozygous *Tor*^{2L1} allele was not strong
263 enough for us to detect a requirement for Tor in ribosomal biogenesis. Therefore, we fed
264 the larvae rapamycin to reduce Tor signaling (Fig. 3M-S). In both control and rapamycin-
265 fed animals, the blastema cells had larger nucleoli than cells in the hinge (Fig. 3M,P).
266 Interestingly, the rapamycin-fed animals had smaller nucleoli in the blastema compared
267 to those in larvae fed control food (Fig. 3N,Q,S). Thus, Tor signaling is important for
268 ribosome biogenesis.
269
270 **Crosstalk between Tor signaling and Myc in the regeneration blastema**
271 Several studies have shown interactions between Myc and Tor in regulating growth in
272 *Drosophila* (Kuo et al., 2015; Parisi et al., 2011; Teleman et al., 2008). Thus, we asked
273 whether there is also a crosstalk between Myc and Tor in the regeneration blastema. First,
274 we asked whether regenerating discs with reduced Myc have reduced Tor activity by
275 immunostaining for p-S6 in *Myc*^{P0}/*Y* regenerating discs and found reduced p-S6 intensity
276 (Fig. S3O-P'). Thus, Myc is important for increased Tor signaling in the regeneration
277 blastema.
278
279 Next, we asked if reduced Tor activity would reduce Myc expression in the regeneration
280 blastema. We used rapamycin feeding to inhibit Tor activity and the *Myc-lacZ* reporter
281 line to examine Myc transcription. We saw reduced transcription of the Myc reporter in
282 the animals fed with rapamycin, compared to the animals fed with control food (Fig. S3R-
283 T), suggesting that Tor signaling regulates Myc expression. Together, these results
284 establish the existence of crosstalk between Myc and Tor signaling in the regeneration
285 blastema.

286

287 **Mapping the domain of high Myc expression in the regeneration blastema**

288 Two sets of scRNA-seq data from regenerating *Drosophila* wing imaginal discs identified
289 cells belonging to the regeneration blastema: called blastema 1 and blastema 2 cells
290 (Worley et al., 2022), or wound alpha cells (Floc'hlay et al., 2023). The ablation assays
291 used in these two studies were slightly different; we used the pro-apoptotic gene *reaper*
292 to induce cell death whereas these studies used the TNFα *eiger*. In addition, Floc'hlay et
293 al. activated ablation for 40 hours instead of the 24 hours that we and Worley et al. used.
294 Therefore, to confirm that the expression of the blastema markers in our ablation system
295 is similar to those identified in these reports, we used Upd3, a JAK/STAT ligand, as a
296 blastema 1 marker and Wg as a blastema 1 and 2 marker (Worley et al., 2022). To
297 visualize *upd3* expression, we used the reporter line *upd3-lacZ* (Bunker et al., 2015). In
298 regenerating wing discs, we confirmed two zones in the regeneration blastema, in which
299 the Wg-expressing area was larger than the *upd3-lacZ*-expressing area (Fig. 4 A-B'),
300 confirming the existence of blastema 1 and 2 cells in our discs. To understand where Myc
301 is upregulated, we used Wg as a blastema marker and co-immunostained for Myc. While
302 Wg did not co-localize with Myc in an undamaged disc (Fig. 4C), in R24 discs, high Myc
303 expression coincided with high Wg expression as previously reported (Smith-Bolton et al.,
304 2009)(Fig. 4D-D').

305

306 We also determined the extent to which the blastema as defined by Worley et al.
307 coincided with Nubbin (Nub) expression, which is normally found in the wing pouch and
308 overlaps with the inner ring of Wg at the boundary between the pouch and the hinge (Ng
309 et al., 1995; Terriente et al., 2008). In an undamaged wing disc, the Nub-expressing area
310 was slightly larger than the moderate Myc-expressing area (Fig. 4E). During regeneration,
311 the Nub-expressing area was also larger than the high Myc-expressing area (Fig. 4F-F').
312 Therefore, the blastema as defined by Wg and Myc expression is smaller than the Nub-
313 expressing area. To determine which cells in the regenerating disc were hinge cells and
314 if there is any overlap between the hinge and the regeneration blastema, we used a Zfh2
315 antibody (Tran et al., 2010) (Fig. 4G-H') and the JAK/STAT signaling reporter
316 *10XSTAT92E-GFP* (Bach et al., 2007) (Fig. 4I-J') as hinge markers. In both undamaged

317 (Fig. 4G,I) and damaged discs (Fig. 4H-H',J-J'), the hinge markers were expressed
318 directly adjacent to, but not overlapping with, the zone with elevated Myc expression.
319
320 To ask whether Nub and Zfh2 expression overlapped in regenerating discs, we used the
321 *nub-MiMIC-GFP* (*nub*^{MI05126}) line, in which a MiMIC transposable element inserted into
322 the *nub* locus expresses GFP in cells that are also marked with anti-Nub immunostaining
323 (Khan et al., 2017; Venken et al., 2011b). In undamaged wing discs, Nub-GFP expression
324 overlapped with Zfh2-positive cells at the inner ring of Wg expression (Fig. 4K), consistent
325 with previous studies (Terriente et al., 2008). In regenerating wing discs, we also found
326 Nub-GFP expression overlapping with Zfh2 expression (Fig. 4L). Furthermore, Wg, Nub,
327 and Zfh2 expression together showed that the blastema was smaller than the Nub-
328 expressing area but directly adjacent to the cells expressing both Nub and the hinge
329 markers (Fig. 4L,L"). Interestingly, hinge cells adjacent to the blastema are flexible in their
330 identity and can become pouch cells during re-growth (Herrera et al., 2013; Ledruet al.,
331 2022; Worley et al., 2018), which may be occurring in the Nub-expressing (Nub+) Zfh2+
332 zone. Thus, the high Myc-expressing zone colocalized with the blastema as defined by
333 single-cell sequencing and did not overlap with hinge cells.
334
335 **The regeneration blastema includes additional zones of elevated growth outside**
336 **the canonical blastema**
337 While immunostaining for p-S6, we marked the blastema by immunostaining for Wg and
338 found that the region with elevated Tor activity was larger than the area with Wg
339 expression (Fig. 3A). In addition, the region marked with the OPP translation assay was
340 also larger than the Wg-expressing area (Fig. 3J'). Thus, we sought to better understand
341 the spatial relationships among the blastema, Myc expression, Tor signaling, and
342 enhanced translation. Given that anti-Myc and anti-p-S6 are both rabbit antibodies, and
343 that Myc and Wg expression co-localized, we used the Wg antibody to mark the Myc-
344 expressing blastema cells. By visualizing Wg, p-S6, and translation, we discovered
345 additional concentric zones of the regeneration blastema. Wg, marking the canonical
346 blastema, was expressed in the center, which we call Growth Zone A (Fig. 5A,B), and
347 which also had elevated p-S6 and OPP signal (Fig. 5C,D). Growth Zone B, the area

348 outside of Zone A, had high p-S6 but not Wg (Fig. 5A,C-E). Growth Zone C was the area
349 with high translation but not upregulated Wg, Myc, or p-S6 (Fig. 5A,F-G). To confirm the
350 existence of these zones, we quantified the area of each (Fig. 5H,I) and examined the
351 fluorescence intensity profile of a cross-section through the wing disc (Fig. S5A-G'). Both
352 analyses indicated that there were three distinct zones within the regeneration blastema.
353
354 We wondered whether the OPP signal in Zone C that extended beyond Zone B was
355 caused by Tor signaling non-autonomously inducing increased translation, or by spread
356 of the OPP signal, or by an unknown additional factor that increases translation. To test
357 the extent to which Tor activity can induce OPP signal non-autonomously, we activated
358 Tor in the posterior half of an undamaged wing disc using *hhGal4, UAS-Tsc2RNAi*
359 (*hh>Tsc2i*) and performed the OPP assay and p-S6 immunostaining (Fig. S5H-Q). The
360 elevated OPP signal extended beyond the A/P boundary while the p-S6 immunostaining
361 did not (Fig. S5H-Q). Therefore, Tor activity can induce elevated translation in the
362 adjacent cells or the OPP assay signal spreads, perhaps due to newly synthesized
363 secreted or extracellular proteins labeled with OPP.
364
365 To determine whether Growth Zone C coincided with the Nub-expressing area, we
366 combined the OPP assay with Nub immunostaining (Fig. 5J-L). The Nub+ area was
367 slightly larger than the area with elevated translation, indicating that Growth Zone C is
368 smaller than the remaining inner hinge (Fig. 5J-L).
369
370 **The concentric growth zones have different proliferation rates**
371 We wondered whether these blastema zones were biologically relevant. Therefore, we
372 asked if cell proliferation was different across these zones. Given that anti-PH3 and anti-
373 p-S6 are both rabbit antibodies, we could not use p-S6 to mark Zone B. Therefore, we
374 took an approximate approach by measuring the area of each zone and calculating the
375 average radius. We used the radii to determine the distances between the edges of
376 Growth Zones A, B, and C. Using these measurements, the average distance between
377 the edges of Growth Zone A and B was 13 microns, and the average distance between
378 the edges of Growth Zone B and C was 16 microns (Fig. 5A,I). We then immunostained

379 for Wg to establish the boundary of Growth Zone A, and measured concentric zones
380 based on the shape of Wg immunostaining (Fig. 5M). We then assessed mitoses per area
381 in each zone (Fig. 5N). Proliferation was highest in Growth Zone A, was slightly reduced
382 in Growth Zone B, and was even lower in Growth Zone C. Proliferation in the cells 10
383 microns outside of Growth Zone C was even lower. Thus, these growth zones are
384 biologically meaningful and contribute at different levels to the regrown wing pouch.
385
386 **Myc expression induces cell death at the periphery of Growth Zone A**
387 Given the difference in Myc levels between Growth Zone A and the rest of the disc, we
388 wondered whether cell competition was occurring. We quantitated cell death using the
389 terminal d-UTP nick-end labeling (TUNEL) assay. Since we used apoptosis to induce
390 tissue damage, we needed to distinguish between ablation and cell competition. We used
391 *UAS-eGFP* to mark apoptotic cells eliminated by our ablation system. At R0, GFP-
392 expressing debris was found on both the basal and the apical sides of the columnar
393 epithelium, or disc proper (Fig. 6A). However, at R24, the GFP-containing debris on the
394 basal side of the epithelium was mostly gone (Fig. 6B), and most of the TUNEL-positive
395 cells did not express GFP (Fig. 6B).
396
397 Cells undergoing apoptosis due to cell competition are extruded toward the basal side of
398 the epithelium (Amoyel and Bach, 2014; Li and Baker, 2007). In addition, cell death driven
399 by Myc-induced super competition occurs within an eight-cell zone adjacent to the winner
400 cells (De La Cova et al., 2004). To set a baseline for quantification, we quantified TUNEL
401 in a negative control, in which *dpp-Gal4* was used to drive *UAS-GFP* in a normally
402 developing wing disc, and a positive control, in which *dpp-Gal4* was used to drive *UAS-*
403 *Myc*. In the negative control, there was no Myc expression difference and no TUNEL-
404 positive cells (Fig. 6C,C',G). In the positive control, cell death was observed in cells
405 located inside the high-Myc stripe and in cells located within an eight-cell region adjacent
406 to the high-Myc cells (Fig. 6D,D',G). These results concurred with previous studies (De
407 La Cova et al., 2004) and gave us a baseline for measuring cell competition due to
408 elevated Myc expression.
409

410 We then quantified TUNEL-positive cells in regenerating discs that were on the basal side
411 of the epithelium within an eight-cell-wide band outside of the Myc-expressing cells (Fig.
412 6E,E'). We found cell death at the basal side of regenerating wing discs that was even
413 higher than in the positive controls (Fig. 6E-E',G). To determine whether this apoptosis
414 was due to elevated Myc expression, we quantified TUNEL-positive cells in *Myc*^{P0}
415 regenerating discs (Fig. 6F,F',G). Surprisingly, the overall number of TUNEL-positive
416 cells on the basal side of the epithelium was not reduced in *Myc*^{P0} regenerating discs (Fig.
417 6G). However, the number of TUNEL-positive cells inside of the Wg+ zone in *Myc*^{P0} discs
418 was higher (Fig. 6H,I) and cell death at the periphery of the Wg+ zone was significantly
419 reduced (Fig. 6H,J). This finding suggests that the cell death observed outside of the Wg+
420 and Myc+ zone is due to Myc expression level differences. Furthermore, the increased
421 cell death within the Wg+ zone in *Myc*^{P0} regenerating discs suggested that Myc is
422 important for survival of these blastema cells. The blastema is subject to complex
423 signaling interactions due to the damage response, which may lead to this requirement
424 for elevated Myc for cell survival.
425

426 **Cell competition induced in regenerating wing discs is distinct from experimentally**
427 **induced cell competition**

428 Cell competition and super-competition studies usually involve genetic clones that differ
429 by one or two factors relative to the surrounding cells, experimentally establishing a
430 mismatch in cell fitness. However, in regenerating imaginal discs, there are overlapping
431 and adjacent zones of elevated Wg, JAK/STAT, Yki, JNK, p38, and Tor signaling
432 (Bergantiños et al., 2010; Grusche et al., 2011; Santabárbara-Ruiz et al., 2015; Smith-
433 Bolton et al., 2009; Sun and Irvine, 2011) (Figs. 4C-D',I-J', 5B,E), which may render
434 fitness comparisons during regeneration more complex than the binary comparisons
435 made in cell competition studies. Therefore, to ask whether the cells outside the high Myc
436 zone were behaving like "loser cells", we examined three different factors that are
437 important for loser cell fate in cell competition and super-competition, including
438 proteotoxic stress, autophagy, and expression of Xrp1.
439

440 The distinction between cell competition and super-competition is based on whether wild-
441 type cells are winner cells or loser cells (Morata, 2021). However, it is unclear whether
442 the cells outside of the high-Myc zone in regenerating discs can be described as wild-
443 type cells because Myc levels are lower than in normal discs. In addition, Myc levels in
444 the blastema are elevated relative to the rest of the disc and relative to undamaged discs
445 but are not as high as when Myc is overexpressed. Given that loser cells during cell
446 competition have increased eIF2α phosphorylation due to proteotoxic stress
447 (Baumgartner et al., 2021; Kiparaki et al., 2022), and winner cells during super-
448 competition also have increased eIF2α phosphorylation due to proteotoxic stress (Paul et
449 al., 2024), we examined p-eIF2α levels in regenerating discs to determine which type of
450 cell competition was occurring.
451
452 In an undamaged wing disc eIF2α was phosphorylated throughout the disc (Fig. 7A). After
453 tissue damage, phosphorylation of eIF2α was reduced in the Wg+ zone of the
454 regeneration blastema (Fig. 7B-B'). Therefore, the enhanced translation in the blastema
455 did not cause proteotoxic stress, and the regenerating disc may be experiencing
456 something closer to cell competition and not super-competition.
457
458 Cell elimination due to cell competition can involve an increase in autophagy (Nagata et
459 al., 2019). Therefore, we used the autophagy marker *Atg8a-mcherry* (Hegedűs et al.,
460 2016; Mauvezin et al., 2014) and counted mCherry-positive puncta in the cells directly
461 adjacent to the Wg+ zone (the boundary) and in the cells within the eight-cell perimeter
462 outside of the Wg+ zone (Fig. 7C-E). While there were few or no mCherry-positive puncta
463 in undamaged wing discs (Fig. 7C), mCherry-positive puncta were observed in
464 regenerating wing discs (Fig. 7D), particularly at the boundary and in the cells within the
465 8-cell perimeter outside of the Wg+ zone (Fig. 7E).
466
467 Xrp1 is a basic leucine zipper domain (bZIP) protein that is expressed in loser cells and
468 is essential for loser cell elimination during imaginal disc cell competition (Baillon et al.,
469 2018; Kiparaki et al., 2022; Lee et al., 2018; Ochi et al., 2021). We did not detect
470 expression level differences between the cells inside the blastema and the cells

471 surrounding the blastema using an Xrp1 antibody (Brown et al., 2021) (Fig. 7F-G) an
472 *Xrp1-GFP* in which the Xrp1 protein is tagged with GFP (Fig. S6A-A")(Kudron et al., 2018),
473 or an enhancer trap line *Xrp1-lacZ*^{02515} (Bellen et al., 2004). (Fig. 7H-I). Therefore, the cell
474 death surrounding the high Myc area in the blastema might not be mediated through *Xrp1*.
475
476 To confirm that cell death surrounding the high-Myc area is not mediated by *Xrp1*, we
477 examined cell death in regenerating wing discs that were heterozygous for the mutant
478 *Xrp1*$^{m2-73}$, which is a truncated allele that eliminates cell competition when heterozygous
479 (Lee et al., 2016; Lee et al., 2018). Cell death surrounding the Wg+ blastema zone was
480 not reduced in *Xrp1*$^{m2-73}$/+ discs (Fig. 7J-K). Given that Xrp1 is not differentially expressed,
481 and that heterozygous *Xrp1* does not rescue the cell death at the periphery of the
482 blastema, it is unlikely that Xrp-1 mediates this Myc-induced cell death.
483
484 The data above suggested that increased Myc in the regeneration blastema led to
485 something closer to cell competition than super-competition. Additionally, Myc-induced
486 cell death outside the high-Myc zone is not identical to canonical cell competition, which
487 is mediated by Xrp1. Therefore, we conclude that the cell death seen around the Wg+,
488 high-Myc blastema zone does not fall neatly into either the classic cell competition or
489 super-competition categories.
490
491 **Discussion**
492 We have shown that Myc and Tor are two critical factors that regulate regenerative growth.
493 Reduction of either Myc expression or Tor kinase activity impaired proliferation and
494 translation in the regeneration blastema. Furthermore, our findings revealed concentric
495 growth zones that extend beyond the blastema as defined by transcriptional profiling. We
496 also demonstrated that the upregulated Myc expression induces cell competition-like cell
497 death in the surrounding cells.
498
499 In our concentric growth zone model, the growth zones were differentiated through
500 expression of genes such as Wg and Myc, activated Tor signaling, and elevated
501 translation. Given that the shape of each zone is similar, it is likely that some secreted

502 factor in Growth Zone A establishes the outer zones, perhaps through damage-response
503 signaling such as reactive oxygen species, morphogen signaling such as Wg, or
504 mechanical signaling such as the Hippo pathway. Furthermore, the high translation in
505 Zone C may be a non-autonomous effect of high Tor activity in Zone B. Given that these
506 distinct zones were not identified by scRNA-seq experiments (Floc'hlay et al., 2023;
507 Worley et al., 2022), it is unlikely that cells in Zones B and C have differential gene
508 expression. Importantly, the differences in proliferation across the zones indicate that their
509 underlying biological differences impact their contribution to regeneration.
510
511 Interestingly, the enhanced Myc expression in the regeneration blastema has a double-
512 edged effect on the regenerating wing disc. While Myc drives regrowth in Growth Zone A,
513 it also induces cell death in the neighboring cells, which includes Growth Zones B and C,
514 tempering their ability to contribute to the regenerated tissue. Although this cell death was
515 mediated by Myc, with proteotoxic stress reduced in the winner cells and autophagy
516 increased in the loser cells, the loser cells did not upregulate Xrp1. Thus, these
517 interactions did not completely resemble cell competition as described in previous studies.
518 Notably, while Growth Zone A cells had high Myc expression and thus were winner cells,
519 the cells outside of Growth Zone A still had elevated translation. In addition, JAK/STAT
520 signaling was also high outside of growth Zone A, and JAK/STAT signaling can both
521 induce cell competition and recue loser cell death (Rodrigues et al., 2012). Furthermore,
522 JNK signaling, Yki activity, and mechanical stress can also influence cell competition
523 (Baker, 2020; Morata, 2021). Indeed, regeneration occurs in a more complex signaling
524 milieu than classical cell competition experiments and may provide clues to how cell
525 competition operates in other complex microenvironments such as tumors. Furthermore,
526 our work presents the first evidence of endogenous cell competition in a non-stem cell-
527 based regeneration model, further exploration of which will enhance our understanding
528 of both regeneration and cell competition.
529
530 **Materials and Method**
531 **Tissue ablation**

532 Ablation experiments were performed as previously described (Smith-Bolton et al., 2009).
533 Briefly, egg lays were performed at 25°C in the dark for 4 hours, then incubated at 18°C.
534 First-instar larvae were picked on day 2 and placed in vials, 50 larvae/vial. On day 7, vials
535 were incubated for 24 hours in a 30°C circulating water bath, kept on ice for 5 minutes to
536 reduce the temperature, then returned to the 18°C incubator *Myc*^{P0} animals had ablation
537 induced 4 hours later to coincide with the early third instar stage because they have
538 delayed development (Abidi et al., 2023).
539

540 **Drosophila strains**

541 Fly lines used were: *w*^{1118} (Hazelrigg et al., 1984); *w*^{1118}*; rnGal4*, *UAS-*
542 *rpr*, *tubGal80ts/TM6B*, *tubGal80* (Smith-Bolton et al., 2009); *7xEcRE-GFP (Hackney et*
543 *al., 2007; Terry et al., 2024)*(a gift from Kenneth Moberg); *Myc-lacZ* (RRID:BDSC_12247);
544 *Myc*^{P0} (Johnston et al., 1999)(RRID:BDSC_11298); *Tor*^{2L1}(Oldham et al.,
545 2000)(RRID:BDSC_98102); *Upd3-lacZ* (Bunker et al., 2015)(a gift from David Bilder);
546 *10XStat92E-GFP* (Ekas et al., 2006)(RRID:BDSC_26197); Nub-*MiMIC-GFP*
547 (*Mi{MIC}nub*^{MI05126})(Venken et al., 2011a)(RRID:BDSC_37920); *UAS-Myc* (Johnston et
548 al., 1999)(RRID:BDSC_9674); *UAS-GFP* (Shiga et al., 1996)(RRID:BDSC_4775); *Dpp-*
549 *Gal4* (Kojima et al., 2000)(RRID:BDSC_93385); *Xrp1-lacZ* (Bellen et al., 2004)
550 (RRID:BDSC_11569); *Xrp1-GFP* (Kudron et al., 2018) (RRID:BDSC_83391), *Xrp1*$^{M2-73}$
551 (Lee et al., 2018)(RRID:BDSC_81270); *3xmCherry-Atg8a (Hegedűs et al., 2016)*(a gift
552 from Juhász Gábor).
553

554 **Immunostaining**

555 Immunostaining was carried out as previously described (Smith-Bolton et al., 2009). After
556 dissection, the larval carcasses were fixed in 4% paraformaldehyde (PFA) for 20 minutes
557 at room temperature, followed by 3 washes in 0.1% triton in phosphate-buffered saline
558 (PBS) (0.1% PBST) for 10 minutes. Carcasses were incubated at 4°C overnight in primary
559 antibodies diluted as noted below in 10% normal goat serum and 0.1% PBST, followed
560 by 3 washes of 0.1% PBST for 10 minutes. Secondary antibody was diluted 1:1000 in 10%
561 normal goat serum and 0.1% PBST for incubation at 4°C overnight. After the secondary
562 antibody incubation, the samples were washed 3 times using 0.1% PBST, followed by

563 incubation in 70% glycerol in PBS overnight at 4°C. The wing imaginal discs were then
564 dissected and mounted on slides with Vectashield Anti-fade mounting media (Vector
565 Laboratories, Cat #H-1000).
566
567 Primary antibodies used: anti-Myc (1:250, Santa Cruz Biotechnologies, #sc-28207), anti-
568 p-S6 (Romero-Pozuelo et al., 2017) (1:200, a gift from Aurelio Teleman), anti-phospho-
569 Histone H3 (1:500, Millipore Sigma, #06-570), anti-Nubbin (RRID:AB_2722119) (1:250,
570 Developmental Studies Hybridoma Bank (DSHB), #Nub2D4), anti-Wingless
571 (RRID:AB_528512) (1:100, DSHB, #4D4), anti-Zfh2 (Tran et al., 2010) (1:250, a gift from
572 Chris Doe), anti-β-Galactosidase (1:500, Invitrogen, Thermo Fisher Scientific #A-11132),
573 anti-p-eIF2α (1:100, Cell Signaling, #3398), anti-Xrp1 (Brown et al., 2021) (1:1000, a gift
574 from Hyung Don Ryoo), anti-Fibrillarin (1:100, Abcam, #ab4566). Secondary antibodies
575 were Alexa Fluor 488, 555, 633, 647 (1:1000, Invitrogen) and DAPI (1:1000, Thermo
576 Fisher Scientific #D1306).
577
578 **OPP assay**
579 The OPP assay was conducted as described (Kiparaki and Baker, 2023), using the Click-
580 iT Plus OPP Alexa Fluor 488 Protein Synthesis Assay Kit (Thermo Fisher Scientific,
581 #10456). Briefly, larvae were dissected in Schneider's *Drosophila* Medium (Thermo
582 Fisher Scientific, Cat #21720024) with 10% heat-inactivated fetal bovine serum (Thermo
583 Fisher Scientific, Cat #A3840001). Larval carcasses were incubated with component A at
584 the concentration of 10 μM in Schneider's *Drosophila* Medium with 10% heat-inactivated
585 fetal bovine serum for 15 minutes. After rinsing with PBS, the carcasses were fixed in 4%
586 PFA for 20 minutes, followed by 3 washes for 10 minutes each with 0.1% PBST. After
587 washing, carcasses were blocked in 3% bovine serum albumin (BSA) in PBS for 10
588 minutes before the 30 minutes incubation in the cocktail solution for the click-on reaction.
589 After the reaction, samples were washed with the rinse buffer followed by 2 minutes of
590 blocking in 3% BSA in PBS. Protocols after this step followed the general primary and
591 secondary staining method above.
592
593 **EdU incorporation and detection**

EdU incorporation and detection was carried out as previously described (Gouge and T.W. Christensen, 2010) using the Click-iT EdU kit (Invitrogen, #C10338). Briefly, larvae were dissected in PBS and incubated in EdU at the concentration of 100 μM in Schneider's *Drosophila* Medium for 30 minutes at room temperature, followed by fixation in 4% PFA for 20 minutes, followed by 3 washes of 10 minutes each with 0.1% PBST. After washing, carcasses were blocked in 3% BSA in PBS for 30 minutes before the 30-minute incubation in the cocktail solution for the click-on reaction. Protocols after this step followed the general primary and secondary staining method above.

TUNEL assay

The TUNEL assay was carried out using the *In Situ* Cell Death Detection Kit (Roche, #12156792910). For experiments incorporating the TUNEL assay, we followed the general immunostaining protocol described above. However, for the secondary antibody solution, we used the TUNEL reaction mixture made by mixing the Enzyme Solution and Label Solution at a 1:9 ratio. Secondary antibodies and DAPI were added according to the dilutions listed above. Samples were incubated in this mixture at 4°C overnight, followed by the remainder of the protocol for general immunostaining.

Rapamycin food

Rapamycin (Thermo Fisher Scientific, #AAJ62473MC) was dissolved in ethanol at a 50 mM concentration. The rapamycin solution was added to Nutri-Fly Bloomington food (Genesee Scientific #66-121) to make a 20μM working concentration. For control food, the same amount of ethanol was added. Immediately after the temperature shift in the circulating water bath, larvae were transferred to rapamycin food or control food.

Image acquisition

Discs were imaged on a Zeiss LSM 700, Zeiss LSM 880, or Zeiss LSM 900 confocal microscope. All images for a given experiment were acquired on the same microscope with the same instrument settings. Images were processed using ImageJ (NIH). Maximum intensity projections were created for the confocal images.

625 **Nucleolus measurements**

626 10 nucleoli (anti-Fibrillarin staining) were measured in a 200-pixel x 200-pixel square
627 using ImageJ.

628

629 **Intensity plots**

630 Intensity plots were made using ImageJ. Briefly, a line across the area of interest was
631 selected using the line selection tool, then an intensity plot was generated using the Plot
632 Profile tool.

633

634 **Statistical analysis**

635 All statistical analyses were performed using Welch's t-test on Graphpad Prism. Graphs
636 were made on Graphpad Prism.

637

638 **Acknowledgments**

639 The authors would like to thank Anish Bose, Snigdha Mathure, and Connor Powers for
640 critical reading of the manuscript and helpful discussions. We thank Dr. Kenneth
641 Moberg, Dr. David Bilder, Dr. Chris Doe, Dr. Hyung Don Ryoo, Dr. Aurelio Teleman,
642 and Dr. Juhász Gábor for reagents; the Bloomington Drosophila Stock Center (NIH
643 P40OD018537); the Developmental Studies Hybridoma Bank (NICHD, The University of
644 Iowa); Dr. Glenn Fried, Dr. Duncan Nall, Dr. Umnia Doha, and all the staff at Core
645 Facilities Microscopy suite at the Carl R. Woese Institute for Genomic Biology.

646

647 **Footnotes**

648 **Author contributions**

649 F.T.-Y.H designed, carried out, interpreted the experiments, and prepared the
650 manuscript. R.K.S.-B. designed and interpreted experiments and assisted in preparation
651 of the manuscript.

652

653 **Funding**

654 This work was supported by the National Institutes of Health grants R01GM107140 and
655 R35GM14174 to R.K.S.-B.

Competing interests

The authors declare no competing or financial interests.

Data and resource availability

All relevant data and resource can be found within the article and its supplementary information. In addition, raw data will be posted in the Illinois Databank (insert URL upon acceptance for publication).

838 **Abbott, L. C., Karpen, G. H. and Schubiger, G.** (1981). Compartmental restrictions and blastema formation during
839 pattern regulation in Drosophila imaginal leg discs. *Dev Biol* **87**, 64–75.

840 **Abidi, S. N. F., Hsu, F. T.-Y. and Smith-Bolton, R. K.** (2023). Regenerative growth is constrained by brain tumor to
841 ensure proper patterning in Drosophila. *PLoS Genet* **19**, e1011103.

842 **Alpar, L., Bergantiños, C. and Johnston, L. A.** (2018). Spatially Restricted Regulation of Spätzle/Toll Signaling during
843 Cell Competition. *Dev Cell* **46**, 706-719.e5.

844 **Amoyel, M. and Bach, E. A.** (2014). Cell competition: How to eliminate your neighbours. *Development (Cambridge)*
845 **141**, 988–1000.

846 **Ascanelli, C., Dahir, R. and Wilson, C. H.** (2024). Manipulating Myc for reparative regeneration. *Front Cell Dev Biol*
847 **12**,.

848 **Baillon, L., Germani, F., Rockel, C., Hilchenbach, J. and Basler, K.** (2018). Xrp1 is a transcription factor required for
849 cell competition-driven elimination of loser cells. *Sci Rep* **8**, 17712.

850 **Baker, N. E.** (2020). Emerging mechanisms of cell competition. *Nat Rev Genet* **21**, 683–697.

851 **Baumgartner, M. E., Dinan, M. P., Langton, P. F., Kucinski, I. and Piddini, E.** (2021). Proteotoxic stress is a driver of
852 the loser status and cell competition. *Nat Cell Biol* **23**, 136–146.

853 **Bawa, S., Brooks, D. S., Neville, K. E., Tipping, M., Sagar, M. A., Kollhoff, J. A., Chawla, G., Geisbrecht, B. V,**
854 **Tennessen, J. M., Eliceiri, K. W., et al.** (2020). Drosophila TRIM32 cooperates with glycolytic enzymes to
855 promote cell growth. *Elife* **9**,.

856 **Bellen, H. J., Levis, R. W., Liao, G., He, Y., Carlson, J. W., Tsang, G., Evans-Holm, M., Hiesinger, P. R., Schulze, K. L.,**
857 **Rubin, G. M., et al.** (2004). The BDGP Gene Disruption Project. *Genetics* **167**, 761–781.

858 **Bellosta, P. and Gallant, P.** (2010). Myc Function in Drosophila. *Genes Cancer* **1**, 542–546.

859 **Bergantiños, C., Corominas, M. and Serras, F.** (2010). Cell death-induced regeneration in wing imaginal discs
860 requires JNK signalling. *Development* **137**, 1169–1179.

861 **Blanco, J., Cooper, J. C. and Baker, N. E.** (2020). Roles of C/EBP class bZip proteins in the growth and cell competition
862 of Rp ('Minute') mutants in Drosophila. *Elife* **9**,.

863 **Bosch, M., Serras, F., Martín-Blanco, E. and Baguñà, J.** (2005). JNK signaling pathway required for wound healing in
864 regenerating Drosophila wing imaginal discs. *Dev Biol* **280**, 73–86.

865 **Bosch, M., Bagun, J. and Serras, F.** (2008). Origin and proliferation of blastema cells during regeneration of
866 Drosophila wing imaginal discs. *Int J Dev Biol* **52**, 1043–1050.

867 **Brandão, A. S., Borbinha, J., Pereira, T., Brito, P. H., Lourenço, R., Bensimon-Brito, A. and Jacinto, A.** (2022). A
868 regeneration-triggered metabolic adaptation is necessary for cell identity transitions and cell cycle re-entry to
869 support blastema formation and bone regeneration. *Elife* **11**,.

870 **Brown, B., Mitra, S., Roach, F. D., Vasudevan, D. and Ryoo, H. D.** (2021). The transcription factor Xrp1 is required
871 for PERK-mediated antioxidant gene induction in Drosophila. *Elife* **10**,.

Bunker, B. D., Nellimoottil, T. T., Boileau, R. M., Classen, A. K. and Bilder, D. (2015). The transcriptional response to tumorigenic polarity loss in Drosophila. *Elife* **4**,.

Colombani, J., Andersen, D. S. and Léopol, P. (2012). Secreted peptide dilp8 coordinates Drosophila tissue growth with developmental timing. *Science (1979)* **336**, 582–585.

De La Cova, C., Abril, M., Bellosta, P., Gallant, P. and Johnston, L. A. (2004). Drosophila myc regulates organ size by inducing cell competition. *Cell* **117**, 107–116.

De La Cova, C., Senoo-Matsuda, N., Ziosi, M., Wu, D. C., Bellosta, P., Quinzii, C. M. and Johnston, L. A. (2014). Supercompetitor status of drosophila Myc cells requires p53 as a Fitness sensor to reprogram metabolism and promote viability. *Cell Metab* **19**, 470–483.

Ekas, L. A., Baeg, G.-H., Flaherty, M. S., Ayala-Camargo, A. and Bach, E. A. (2006). JAK/STAT signaling promotes regional specification by negatively regulating *wingless* expression in *Drosophila*. *Development* **133**, 4721–4729.

Floc'hlay, S., Balaji, R., Stanković, D., Christiaens, V. M., Bravo González-Blas, C., De Winter, S., Hulselmans, G. J., De Waegeneer, M., Quan, X., Koldere, D., et al. (2023). Shared enhancer gene regulatory networks between wound and oncogenic programs. *Elife* **12**,.

Fox, D. T., Cohen, E. and Smith-Bolton, R. (2020). Model systems for regeneration: *Drosophila*. *Development* **147**,.

Garelli, A., Gontijo, A. M., Miguela, V., Caparros, E. and Dominguez, M. (2012). Imaginal discs secrete insulin-like peptide 8 to mediate plasticity of growth and maturation. *Science (1979)* **336**, 579–582.

Germani, F., Hain, D., Sternlicht, D., Moreno, E. and Basler, K. (2018). The Toll pathway inhibits tissue growth and regulates cell fitness in an infection-dependent manner. *Elife* **7**,.

Gouge, C. A. and T.W. Christensen (2010). Technique Notes-Detection of S Phase in multiple Drosophila tissues utiliizing the EdU labeling technique. *Drosoph Inf Serv* **93**, 203.

Grewal, S. S., Li, L., Orian, A., Eisenman, R. N. and Edgar, B. A. (2005). Myc-dependent regulation of ribosomal RNA synthesis during Drosophila development. *Nat Cell Biol* **7**, 295–302.

Grusche, F. A., Degoutin, J. L., Richardson, H. E. and Harvey, K. F. (2011). The Salvador/Warts/Hippo pathway controls regenerative tissue growth in Drosophila melanogaster. *Dev Biol* **350**, 255–266.

Hackney, J. F., Pucci, C., Naes, E. and Dobens, L. (2007). Ras signaling modulates activity of the ecdysone receptor EcR during cell migration in the drosophila ovary. *Developmental Dynamics* **236**, 1213–1226.

Hadorn, E. and Buck, D. (1962). Über entwicklungsleistungen transplantierter teilstücke von flügel-imaginalscheiben von Drosophila melanogaster. *Revue suisse de Zoologie*.

Halme, A., Cheng, M. and Hariharan, I. K. (2010). Retinoids Regulate a Developmental Checkpoint for Tissue Regeneration in Drosophila. *Current Biology* **20**, 458–463.

Harris, R. E., Setiawan, L., Saul, J. and Hariharan, I. K. (2016). Localized epigenetic silencing of a damage-activated WNT enhancer limits regeneration in mature Drosophila imaginal discs. *Elife* **5**,.

906 **Harris, R. E., Stinchfield, M. J., Nystrom, S. L., McKay, D. J. and Hariharan, I. K.** (2020). Damage-responsive, maturity-
907 silenced enhancers regulate multiple genes that direct regeneration in drosophila. *Elife* **9**, 1–26.

908 **Hazelrigg, T., Levis, R. and Rubin, G. M.** (1984). Transformation of white locus DNA in Drosophila: Dosage
909 compensation, zeste interaction, and position effects. *Cell* **36**, 469–481.

910 **Hegedűs, K., Takáts, S., Boda, A., Jipa, A., Nagy, P., Varga, K., Kovács, A. L. and Juhász, G.** (2016). The Ccz1-Mon1-
911 Rab7 module and Rab5 control distinct steps of autophagy. *Mol Biol Cell* **27**, 3132–3142.

912 **Herrera, S. C., Martín, R. and Morata, G.** (2013). Tissue Homeostasis in the Wing Disc of Drosophila melanogaster:
913 Immediate Response to Massive Damage during Development. *PLoS Genet* **9**, e1003446.

914 **Jaszczak, J. S. and Halme, A.** (2016). Arrested development: coordinating regeneration with development and
915 growth in Drosophila melanogaster. *Curr Opin Genet Dev* **40**, 87–94.

916 **Jaszczak, J. S., Wolpe, J. B., Dao, A. Q. and Halme, A.** (2015). Nitric Oxide Synthase Regulates Growth Coordination
917 During *Drosophila melanogaster* Imaginal Disc Regeneration. *Genetics* **200**, 1219–1228.

918 **Jaszczak, J. S., Wolpe, J. B., Bhandari, R., Jaszczak, R. G. and Halme, A.** (2016). Growth Coordination During
919 *Drosophila melanogaster* Imaginal Disc Regeneration Is Mediated by Signaling Through the Relaxin Receptor
920 Lgr3 in the Prothoracic Gland. *Genetics* **204**, 703–709.

921 **Johnston, L. A., Prober, D. A., Edgar, B. A., Eisenman, R. N. and Gallant, P.** (1999). Drosophila myc regulates cellular
922 growth during development. *Cell* **98**, 779–790.

923 **Karanja, F., Sahu, S., Weintraub, S., Bhandari, R., Jaszczak, R., Sitt, J. and Halme, A.** (2022). Ecdysone exerts biphasic
924 control of regenerative signaling, coordinating the completion of regeneration with developmental
925 progression. *Proceedings of the National Academy of Sciences* **119**,.

926 **Katsuyama, T., Comoglio, F., Seimiya, M., Cabuy, E. and Paro, R.** (2015). During *Drosophila* disc regeneration,
927 JAK/STAT coordinates cell proliferation with Dilp8-mediated developmental delay. *Proceedings of the National*
928 *Academy of Sciences* **112**,.

929 **Khan, S. J., Abidi, S. N. F., Skinner, A., Tian, Y. and Smith-Bolton, R. K.** (2017). *The Drosophila Duox maturation factor*
930 *is a key component of a positive feedback loop that sustains regeneration signaling*.

931 **Khandekar, A. and Ellis, S. J.** (2024). An expanded view of cell competition. *Development* **151**,.

932 **Kiparaki, M. and Baker, N. E.** (2023). Protocol for assessing translation in living Drosophila imaginal discs by O-
933 propargyl-puromycin incorporation. *STAR Protoc* **4**, 102653.

934 **Kiparaki, M., Khan, C., Folgado-Marco, V., Chuen, J., Moulos, P. and Baker, N. E.** (2022). The transcription factor
935 Xrp1 orchestrates both reduced translation and cell competition upon defective ribosome assembly or
936 function. *Elife* **11**,.

937 **Kojima, T., Sato, M. and Saigo, K.** (2000). Formation and specification of distal leg segments in *Drosophila* by dual
938 *Bar* homeobox genes, *BarH1* and *BarH2*. *Development* **127**, 769–778.

939 **Kudron, M. M., Victorsen, A., Gevirtzman, L., Hillier, L. W., Fisher, W. W., Vafeados, D., Kirkey, M., Hammonds, A.**
940 **S., Gersch, J., Ammouri, H., et al.** (2018). The ModERN Resource: Genome-Wide Binding Profiles for Hundreds
941 of *Drosophila* and *Caenorhabditis elegans* Transcription Factors. *Genetics* **208**, 937–949.

942 **Kuo, Y., Huang, H., Cai, T. and Wang, T.** (2015). Target of rapamycin complex 2 regulates cell growth via Myc in
943 drosophila. *Sci Rep* **5**, 1–10.

944 **Ledru, M., Clark, C. A., Brown, J., Verghese, S., Ferrara, S., Goodspeed, A. and Su, T. T.** (2022). Differential gene
945 expression analysis identified determinants of cell fate plasticity during radiation-induced regeneration in
946 Drosophila. *PLoS Genet* **18**, e1009989.

947 **Lee, C.-H., Rimesso, G., Reynolds, D. M., Cai, J. and Baker, N. E.** (2016). Whole-Genome Sequencing and iPLEX
948 MassARRAY Genotyping Map an EMS-Induced Mutation Affecting Cell Competition in *Drosophila*
949 *melanogaster*. *G3 Genes|Genomes|Genetics* **6**, 3207–3217.

950 **Lee, C.-H., Kiparaki, M., Blanco, J., Folgado, V., Ji, Z., Kumar, A., Rimesso, G. and Baker, N. E.** (2018). A Regulatory
951 Response to Ribosomal Protein Mutations Controls Translation, Growth, and Cell Competition. *Dev Cell* **46**,
952 456-469.e4.

953 **Li, W. and Baker, N. E.** (2007). Engulfment Is Required for Cell Competition. *Cell* **129**, 1215–1225.

954 **Londono, R., Sun, A. X., Tuan, R. S. and Lozito, T. P.** (2018). Tissue Repair and Epimorphic Regeneration: an Overview.
955 *Curr Pathobiol Rep* **6**, 61–69.

956 **Mauvezin, C., Ayala, C., Braden, C. R., Kim, J. and Neufeld, T. P.** (2014). Assays to monitor autophagy in Drosophila.
957 *Methods* **68**, 134–139.

958 **Merino, M. M., Rhiner, C., Lopez-Gay, J. M., Buechel, D., Hauert, B. and Moreno, E.** (2015). Elimination of Unfit
959 Cells Maintains Tissue Health and Prolongs Lifespan. *Cell* **160**, 461–476.

960 **Meyer, S. N., Amoyel, M., Bergantiños, C., De La Cova, C., Schertel, C., Basler, K. and Johnston, L. A.** (2014). An
961 ancient defense system eliminates unfit cells from developing tissues during cell competition. *Science (1979)*
962 **346**,.

963 **Morata, G.** (2021). Cell competition: A historical perspective. *Dev Biol* **476**, 33–40.

964 **Nagata, R., Nakamura, M., Sanaki, Y. and Igaki, T.** (2019). Cell Competition Is Driven by Autophagy. *Dev Cell* **51**, 99-
965 112.e4.

966 **Ng, M., Diaz-Benjumea, F. J. and Cohen, S. M.** (1995). *nubbin* encodes a POU-domain protein required for proximal-
967 distal patterning in the *Drosophila* wing. *Development* **121**, 589–599.

968 **O'Brochta, D. A. and Bryant, P. J.** (1987). Distribution of S-phase cells during the regeneration of Drosophila imaginal
969 wing discs. *Dev Biol* **119**, 137–142.

970 **Ochi, N., Nakamura, M., Nagata, R., Wakasa, N., Nakano, R. and Igaki, T.** (2021). Cell competition is driven by Xrp1-
971 mediated phosphorylation of eukaryotic initiation factor 2α. *PLoS Genet* **17**, e1009958.

972 **Oldham, S., Montagne, J., Radimerski, T., Thomas, G. and Hafen, E.** (2000). Genetic and biochemical
973 characterization of dTOR, the *Drosophila* homolog of the target of rapamycin. *Genes Dev* **14**, 2689–2694.

974 **Parisi, F., Riccardo, S., Daniel, M., Saqcena, M., Kundu, N., Pession, A., Grifoni, D., Stocker, H., Tabak, E. and**
975 **Bellosta, P.** (2011). Drosophila insulin and target of rapamycin (TOR) pathways regulate GSK3 beta activity to
976 control Myc stability and determine Myc expression in vivo. *BMC Biol* **9**, 65.

977 **Paul, P. K., Umarvaish, S., Bajaj, S., S., R. F., Mohan, H., Annaert, W. and Chaudhary, V.** (2024). Maintenance of
978 proteostasis by Drosophila Rer1 is essential for competitive cell survival and Myc-driven overgrowth. *PLoS*
979 *Genet* **20**, e1011171.

980 **Rai, M., Carter, S. M., Shefali, S. A., Chawla, G. and Tennessen, J. M.** (2024). Characterization of genetic and
981 molecular tools for studying the endogenous expression of Lactate dehydrogenase in Drosophila melanogaster.
982 *PLoS One* **19**, e0287865.

983 **Rhiner, C., López-Gay, J. M., Soldini, D., Casas-Tinto, S., Martín, F. A., Lombardía, L. and Moreno, E.** (2010). Flower
984 forms an extracellular code that reveals the fitness of a cell to its neighbors in Drosophila. *Dev Cell* **18**, 985–
985 998.

986 **Rodrigues, A. B., Zoranovic, T., Ayala-Camargo, A., Grewal, S., Reyes-Robles, T., Krasny, M., Christine Wu, D.,**
987 **Johnston, L. A. and Bach, E. A.** (2012). Activated STAT regulates growth and induces competitive interactions
988 independently of Myc, Yorkie, Wingless and ribosome biogenesis. *Development (Cambridge)* **139**, 4051–4061.

989 **Romero-Pozuelo, J., Demetriades, C., Schroeder, P. and Teleman, A. A.** (2017). CycD/Cdk4 and Discontinuities in
990 Dpp Signaling Activate TORC1 in the Drosophila Wing Disc. *Dev Cell* **42**, 376-387.e5.

991 **Santabárbara-Ruiz, P., López-Santillán, M., Martínez-Rodríguez, I., Binagui-Casas, A., Pérez, L., Milán, M.,**
992 **Corominas, M. and Serras, F.** (2015). ROS-Induced JNK and p38 Signaling Is Required for Unpaired Cytokine
993 Activation during Drosophila Regeneration. *PLoS Genet* **11**, e1005595.

994 **Serras, F. and Bellosta, P.** (2024). Drosophila: a Tale of regeneration with MYC. *Front Cell Dev Biol* **12**,.

995 **Shiga, Y., Tanaka-Matakatsu, M. and Hayashi, S.** (1996). A nuclear GFP/β-galactosidase fusion protein as a marker
996 for morphogenesis in living *Drosophila*. *Dev Growth Differ* **38**, 99–106.

997 **Smith-Bolton, R. K., Worley, M. I., Kanda, H. and Hariharan, I. K.** (2009). Regenerative Growth in Drosophila Imaginal
998 Discs Is Regulated by Wingless and Myc. *Dev Cell* **16**, 797–809.

999 **Sun, G. and Irvine, K. D.** (2011). Regulation of Hippo signaling by Jun kinase signaling during compensatory cell
1000 proliferation and regeneration, and in neoplastic tumors. *Dev Biol* **350**, 139–151.

1001 **Swarup, S. and Verheyen, E. M.** (2012). Wnt/Wingless Signaling in Drosophila. *Cold Spring Harb Perspect Biol* **4**,
1002 a007930–a007930.

1003 **Teleman, A. A., Hietakangas, V., Sayadian, A. C. and Cohen, S. M.** (2008). Nutritional Control of Protein Biosynthetic
1004 Capacity by Insulin via Myc in Drosophila. *Cell Metab* **7**, 21–32.

1005 **Terriente, J., Perea, D., Suzanne, M. and Díaz-Benjumea, F. J.** (2008). The Drosophila gene zfh2 is required to
1006 establish proximal-distal domains in the wing disc. *Dev Biol* **320**, 102–112.

1007 **Terry, D., Schweibenz, C. and Moberg, K.** (2024). Local Ecdysone synthesis in a wounded epithelium sustains
1008 developmental delay and promotes regeneration in *Drosophila*. *Development* **151**,.

1009 **Thummel, C. S.** (2001). Molecular Mechanisms of Developmental Timing in C. elegans and Drosophila. *Dev Cell* **1**,
1010 453–465.

1011 **Tran, K. D., Miller, M. R. and Doe, C. Q.** (2010). Recombineering Hunchback identifies two conserved domains
1012 required to maintain neuroblast competence and specify early-born neuronal identity. *Development* **137**,
1013 1421–1430.

1014 **Venken, K. J. T., Schulze, K. L., Haelterman, N. A., Pan, H., He, Y., Evans-Holm, M., Carlson, J. W., Levis, R. W.,**
1015 **Spradling, A. C., Hoskins, R. A., et al.** (2011a). MiMIC: a highly versatile transposon insertion resource for
1016 engineering Drosophila melanogaster genes. *Nat Methods* **8**, 737–43.

1017 **Venken, K. J. T., Schulze, K. L., Haelterman, N. A., Pan, H., He, Y., Evans-Holm, M., Carlson, J. W., Levis, R. W.,**
1018 **Spradling, A. C., Hoskins, R. A., et al.** (2011b). MiMIC: a highly versatile transposon insertion resource for
1019 engineering Drosophila melanogaster genes. *Nat Methods* **8**, 737–743.

1020 **Worley, M. I., Alexander, L. A. and Hariharan, I. K.** (2018). CtBP impedes JNK- and Upd/STAT-driven cell fate
1021 misspecifications in regenerating Drosophila imaginal discs. *Elife* **7**,.

1022 **Worley, M. I., Everetts, N. J., Yasutomi, R., Chang, R. J., Saretha, S., Yosef, N. and Hariharan, I. K.** (2022). Ets21C
1023 sustains a pro-regenerative transcriptional program in blastema cells of Drosophila imaginal discs. *Current*
1024 *Biology* **32**, 3350-3364.e6.

1025

Fig.1

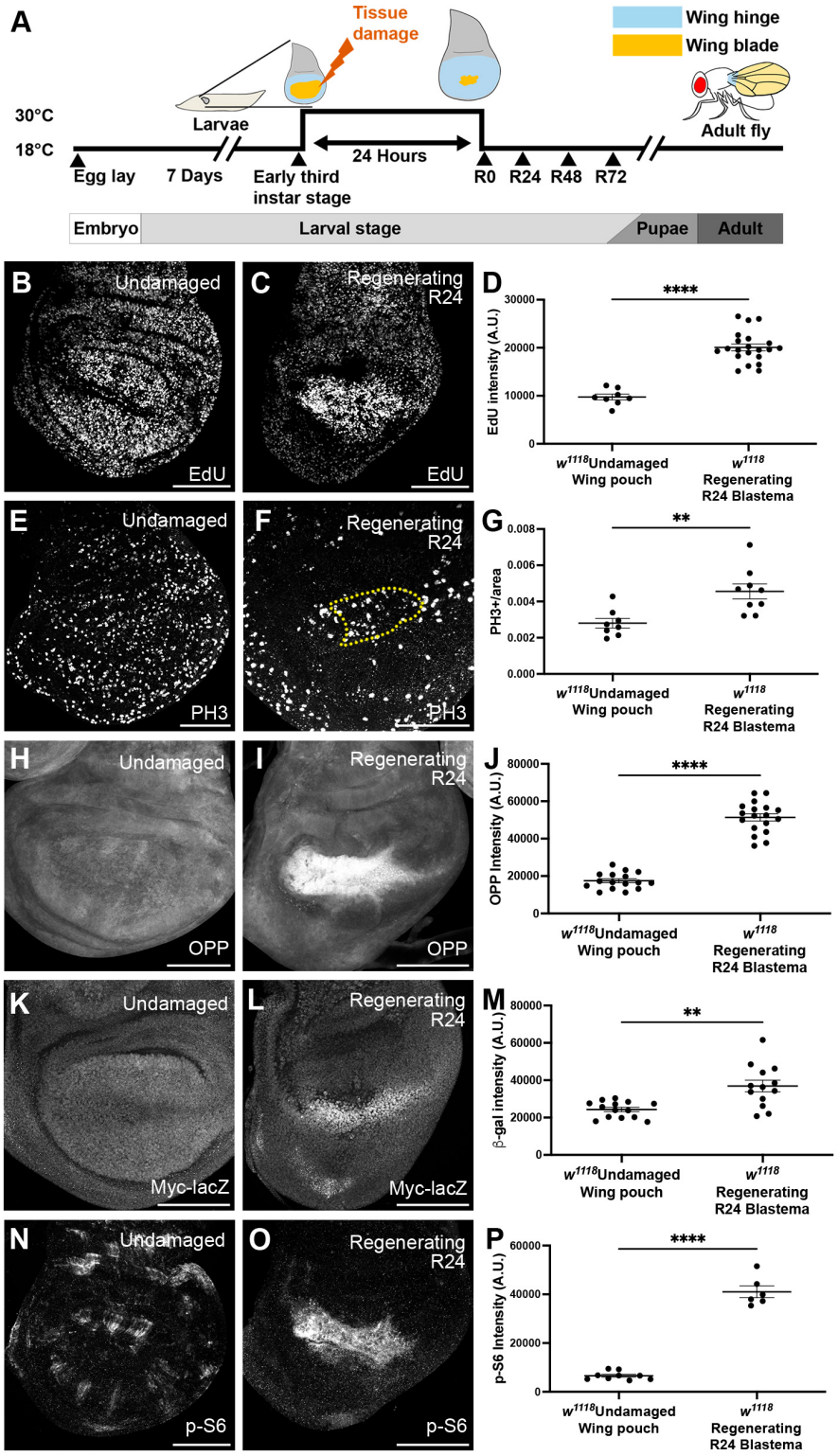
A
Tissue damage
Wing hinge
Wing blade
30°C
18°C
Larvae
Adult fly
24 Hours
Egg lay
7 Days
Early third instar stage
R0
R24
R48
R72
Embryo
Larval stage
Pupae
Adult
B Undamaged EdU
C Regenerating R24 EdU
D
EdU intensity (A.U.)
****
w1118 Undamaged Wing pouch
w1118 Regenerating R24 Blastema
E Undamaged PH3
F Regenerating R24 PH3
G
PH3+/area
**
H Undamaged OPP
I Regenerating R24 OPP
J
OPP intensity (A.U.)
****
K Undamaged Myc-lacZ
L Regenerating R24 Myc-lacZ
M
β-gal intensity (A.U.)
**
N Undamaged p-S6
O Regenerating R24 p-S6
P
p-S6 intensity (A.U.)
****

664 **Figure legends**

665 **Figure 1. Myc expression and Tor signaling in regenerating wing discs**

666 (A) Schematic of the genetic ablation system. (B-C) EdU incorporation marking S-phase
667 cells in an undamaged disc (B) and an R24 disc (C). (D) Quantification of average EdU
668 staining intensity in the wing pouch identified by morphological features. Undamaged
669 n=8, R24 n=21. ****P<0.0001. (E-F) PH3 staining marking mitotic cells in an
670 undamaged disc (E) and an R24 disc (F). (G) Quantification of mitotic cells per area in
671 the wing pouch identified by inner ring of Wg staining (yellow dotted lines in 1F).
672 Undamaged n=8, R24 n=9. **P<0.01. (H-I) OPP assay in an undamaged disc (H) and
673 an R24 disc (I). (J) Quantification of OPP staining intensity in the wing pouch of an
674 undamaged disc or blastema of an R24 disc, identified by the inner ring of Wg staining
675 or Wg staining, respectively. Undamaged n=16, R24 n=18. ****P<0.0001. (K-L) *Myc-*
676 *lacZ* expression detected by β-gal staining in an undamaged disc (K) and an R24 disc
677 (L). (M) Quantification of average β-gal staining intensity in the wing pouch or blastema
678 identified by morphological features. Undamaged n=14, R24 n=13. **P<0.01. (N-O) p-
679 S6 staining in an undamaged disc (N) and an R24 disc (O). (P) Quantification of
680 average p-S6 staining intensity in the wing pouch or blastema identified by Wg staining.
681 Undamaged n=9, R24 n=6. ****P<0.0001. Statistical test used was Welch's t-test. Scale
682 bars are 100μm. Error bars are SEM.

683

Fig. 2

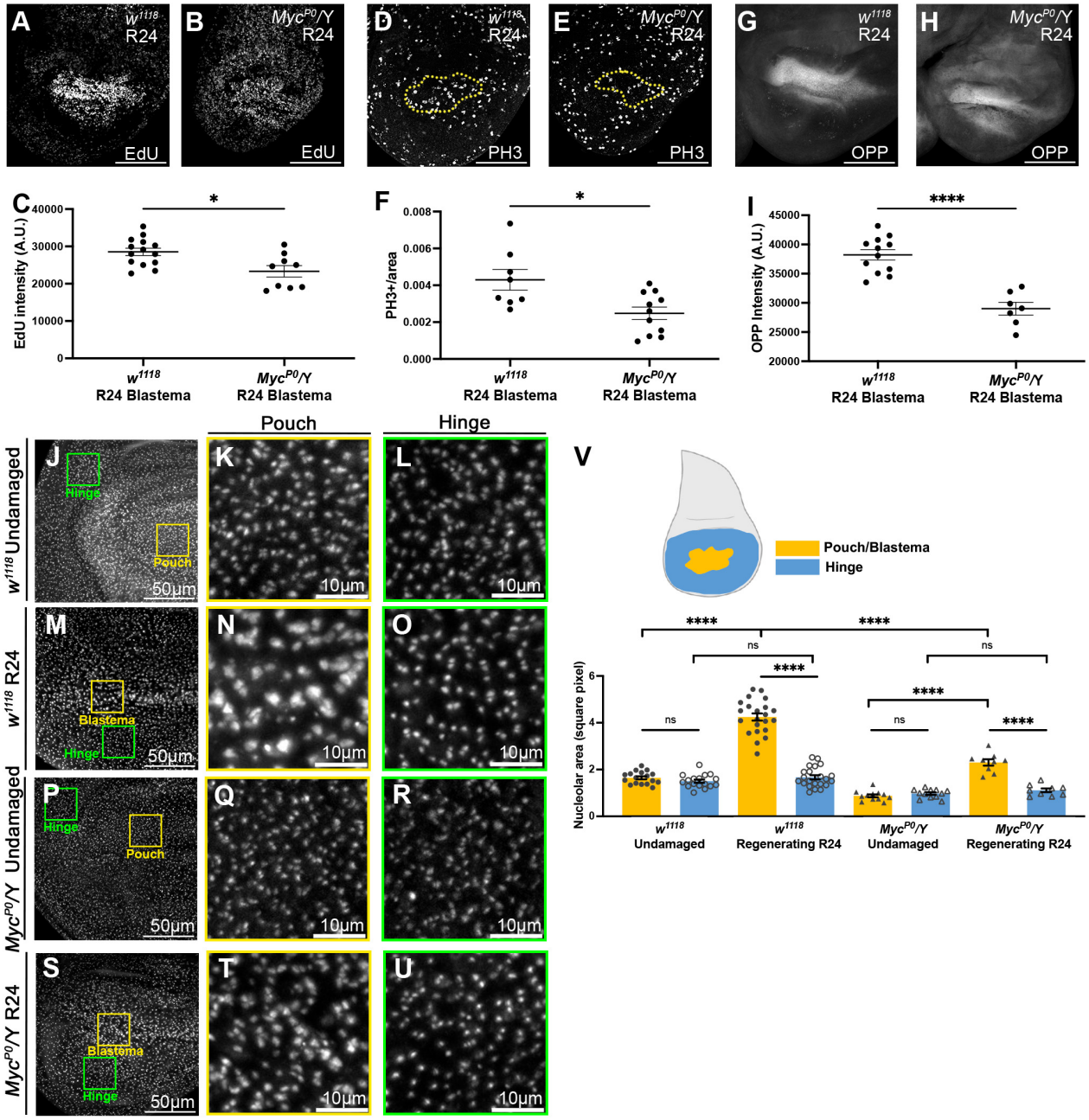
A
w1118
R24
EdU
B
MycP0/Y
R24
EdU
D
w1118
R24
PH3
E
MycP0/Y
R24
PH3
G
w1118
R24
OPP
H
MycP0/Y
R24
OPP
C
EdU intensity (A.U.)
40000
30000
20000
10000
0
*
w1118
R24 Blastema
MycP0/Y
R24 Blastema
F
PH3+/area
0.008
0.006
0.004
0.002
0.000
*
w1118
R24 Blastema
MycP0/Y
R24 Blastema
I
OPP Intensity (A.U.)
45000
40000
35000
30000
25000
20000
****
w1118
R24 Blastema
MycP0/Y
R24 Blastema
Pouch
Hinge
w1118 Undamaged
w1118 R24
MycP0/Y Undamaged
MycP0/Y R24
J
Hinge
Pouch
50µm
K
10µm
L
10µm
M
Blastema
Hinge
50µm
N
10µm
O
10µm
P
Hinge
Pouch
50µm
Q
10µm
R
10µm
S
Blastema
Hinge
50µm
T
10µm
U
10µm
V
Pouch/Blastema
Hinge
Nucleolar area (square pixel)
6
4
2
0
****
****
ns
ns
****
****
ns
****
ns
****
w1118
Undamaged
w1118
Regenerating R24
MycP0/Y
Undamaged
MycP0/Y
Regenerating R24

Figure 2. Myc promotes growth in the regeneration blastema

(A-B) EdU incorporation in a w^{1118} R24 disc (A) and a Myc^{P0}/Y R24 disc (B). (C) Quantification of average EdU intensity in the wing pouch identified by morphological features. w^{1118}n=14, Myc^{P0}/Y n=9. *P<0.05. (D-E) PH3 staining in a w^{1118} R24 disc (D) and a Myc^{P0}/Y R24 disc (E). (F) Quantification of mitotic cells per area in the blastema (Wg, yellow dotted lines in D-E). w^{1118} n=8, Myc^{P0}/Y n=11. *P<0.05. (G-H) OPP assay in a w^{1118} R24 disc (G) and a Myc^{P0}/Y R24 disc (H). (I) Quantification of average OPP signal in the Wg+ blastema. w^{1118} n=12, Myc^{P0}/Y n=7. ****P<0.0001. (J-U) Fibrillarin staining marking nucleoli in a w^{1118} undamaged disc (J-L), a w^{1118} R24 disc (M-O), a Myc^{P0}/Y undamaged disc (P-R), and a Myc^{P0}/Y R24 disc (S-U). (K,N,Q,T) 200-pixel square from pouch or Wg+ blastema (yellow boxes). (L,O,R,U) 200-pixel square from hinge (green boxes). (V) Quantification of nucleolus size. w^{1118} undamaged n=17, w^{1118} R24 n=22, Myc^{P0}/Y undamaged n=12, Myc^{P0}/Y R24 n=9. n.s. P>0.05, ****P<0.0001. Statistical test used was Welch's t-test. Scale bars are 100μm. Error bars are SEM.

Fig. 3

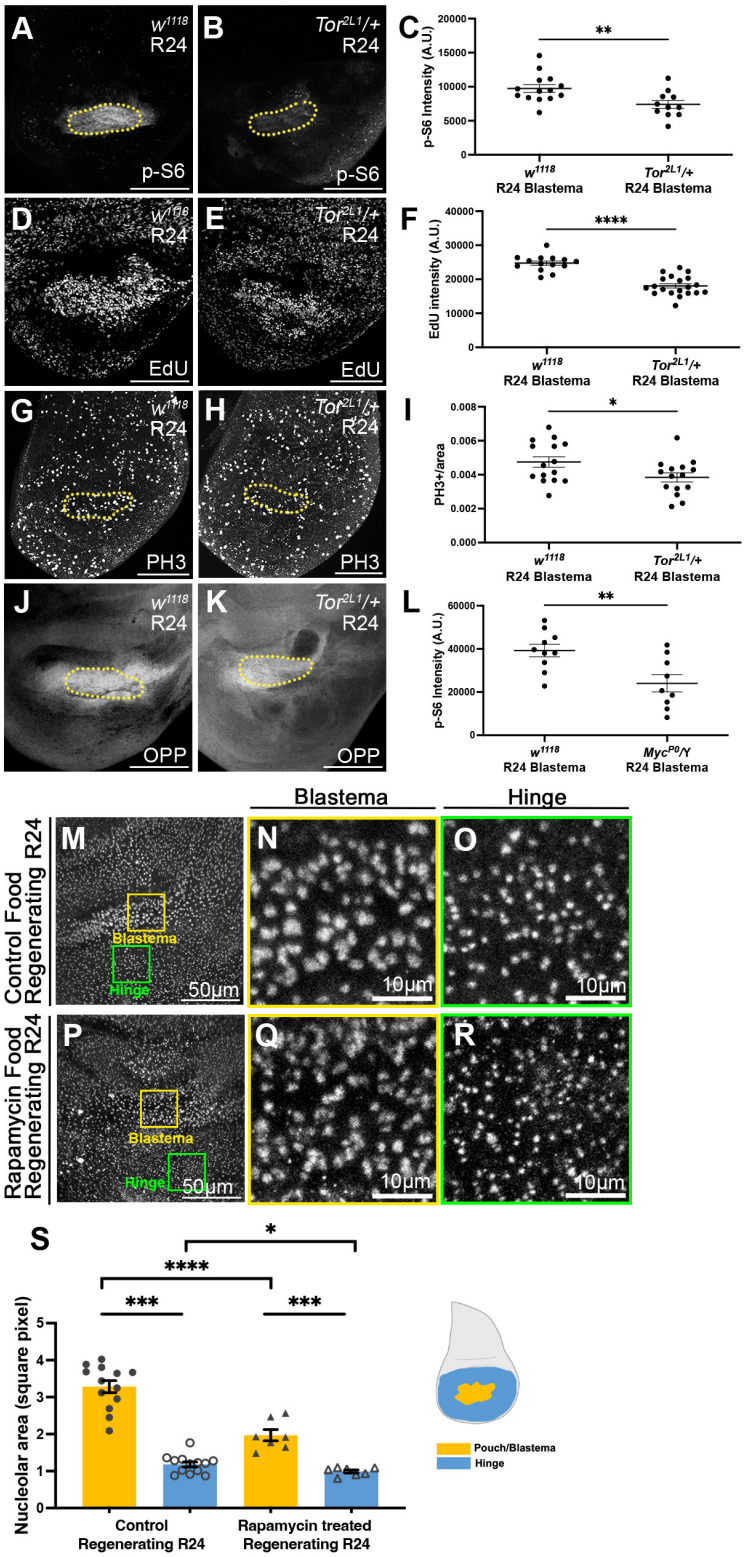
A
w1118
R24
p-S6
B
Tor2L1/+
R24
p-S6
C
p-S6 Intensity (A.U.)
**
w1118
R24 Blastema
Tor2L1/+
R24 Blastema
D
w1118
R24
EdU
E
Tor2L1/+
R24
EdU
F
EdU intensity (A.U.)
****
w1118
R24 Blastema
Tor2L1/+
R24 Blastema
G
w1118
R24
PH3
H
Tor2L1/+
R24
PH3
I
PH3+/area
*
w1118
R24 Blastema
Tor2L1/+
R24 Blastema
J
w1118
R24
OPP
K
Tor2L1/+
R24
OPP
L
p-S6 Intensity (A.U.)
**
w1118
R24 Blastema
MycP0/Y
R24 Blastema
Blastema
Hinge
Control Food
Regenerating R24
M
Blastema
Hinge
50µm
N
10µm
O
10µm
Rapamycin Food
Regenerating R24
P
Blastema
Hinge
50µm
Q
10µm
R
10µm
S
Nucleolar area (square pixel)
*
****
***
***
Control
Regenerating R24
Rapamycin treated
Regenerating R24
Pouch/Blastema
Hinge

Figure 3. Tor promotes growth in the regeneration blastema

(A-B) p-S6 immunostaining in a w^{1118} R24 disc (A) and a Tor^{2L1}/+ R24 disc (B). (C) Quantification of average p-S6 staining intensity in the Wg+ blastema (yellow dotted lines). w^{1118} n=14, Tor^{2L1}/+ n=11. **P<0.01, Welch's t-test. (D-E) EdU incorporation in a w^{1118} R24 disc (D) and a Tor^{2L1}/+ R24 disc (E). (F) Quantification of average EdU staining intensity in the blastema identified by morphological features. w^{1118} n=14, Tor^{2L1}/+ n=20. ****P<0.0001. (G-H) PH3 staining in a w^{1118} R24 disc (G) and a Tor^{2L1}/+ R24 disc (H). (I) Quantification of mitotic cells per area in the Wg+ blastema (yellow dotted lines). w^{1118} n=15, Tor^{2L1}/+ n=15. *P<0.05. (J-K) OPP assay in a w^{1118} R24 disc (J) and a Tor^{2L1}/+ R24 disc (K). (L) Quantification of average OPP staining in the Wg+ blastema (yellow dotted lines). w^{1118} n=16, Tor^{2L1}/+ n=16. ***P<0.001. (M-S) Fibrillarin staining in an R24 disc after feeding with control food (M-O) or food containing rapamycin (P-R). (N,Q) 200-pixel squares from the Wg+ blastema (yellow boxes). (O,R) 200-pixel square from the hinge (green boxes). (S) Quantification of nucleolus size in hinge and blastema. control n=13, rapamycin n=7. *P<0.05, ***P<0.001, ****P<0.0001.

Fig. 4

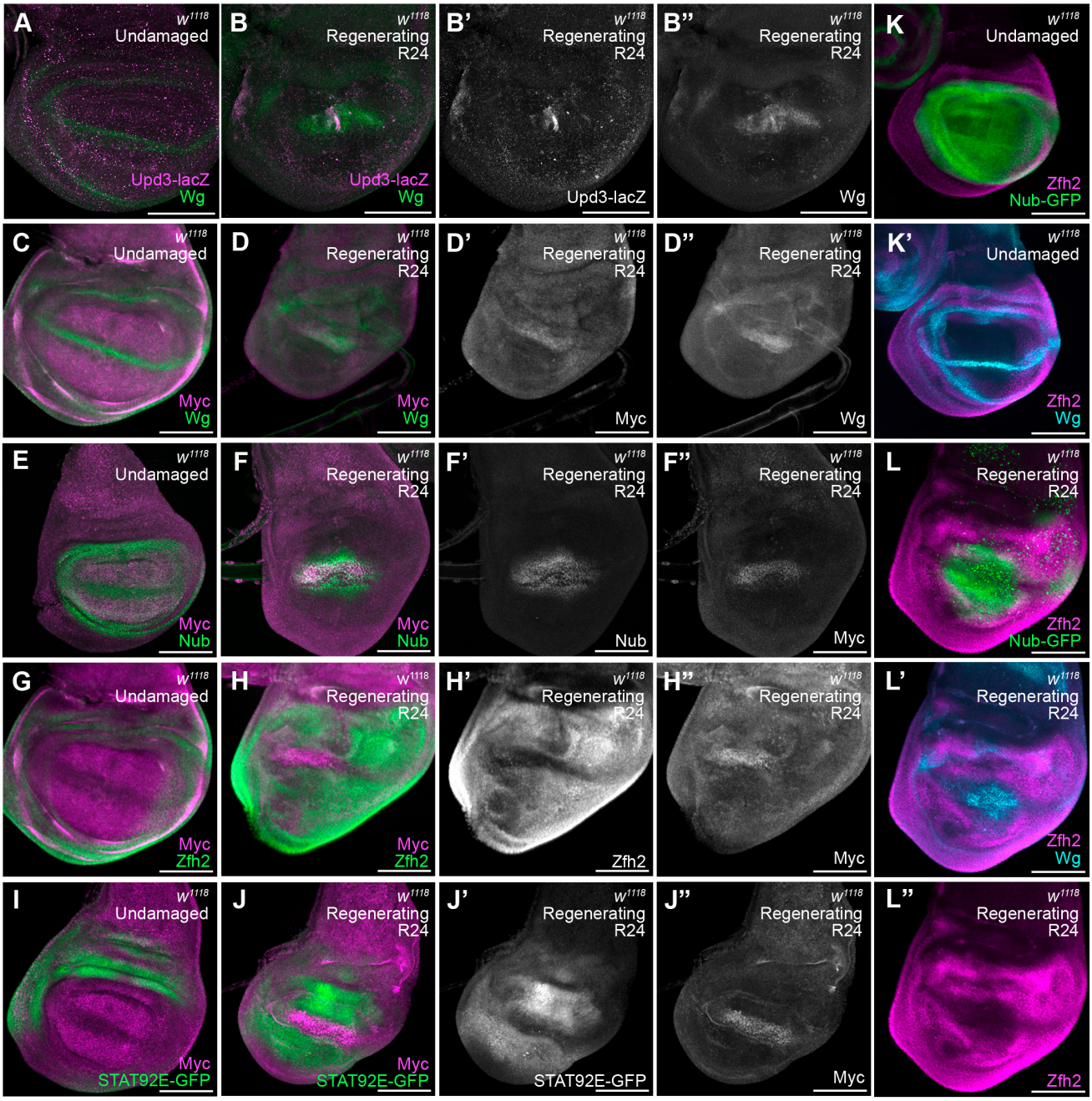
A
w1118
Undamaged
Upd3-lacZ
Wg
B
w1118
Regenerating
R24
Upd3-lacZ
Wg
B'
w1118
Regenerating
R24
Upd3-lacZ
B''
w1118
Regenerating
R24
Wg
K
w1118
Undamaged
Zfh2
Nub-GFP
C
w1118
Undamaged
Myc
Wg
D
w1118
Regenerating
R24
Myc
Wg
D'
w1118
Regenerating
R24
Myc
D''
w1118
Regenerating
R24
Wg
K'
w1118
Undamaged
Zfh2
Wg
E
w1118
Undamaged
Myc
Nub
F
w1118
Regenerating
R24
Myc
Nub
F'
w1118
Regenerating
R24
Nub
F''
w1118
Regenerating
R24
Myc
L
w1118
Regenerating
R24
Zfh2
Nub-GFP
G
w1118
Undamaged
Myc
Zfh2
H
w1118
Regenerating
R24
Myc
Zfh2
H'
w1118
Regenerating
R24
Zfh2
H''
w1118
Regenerating
R24
Myc
L'
w1118
Regenerating
R24
Zfh2
Wg
I
w1118
Undamaged
Myc
STAT92E-GFP
J
w1118
Regenerating
R24
Myc
STAT92E-GFP
J'
w1118
Regenerating
R24
STAT92E-GFP
J''
w1118
Regenerating
R24
Myc
L''
w1118
Regenerating
R24
Zfh2

717 **Figure 4. Mapping the domain of Myc expression in the regeneration blastema**
718 (A-B”) Wg immunostaining and *upd-lacZ* expression detected by β-Gal immunostaining
719 in an undamaged disc (A) and an R24 disc (B-B”). (C-D”) Myc and Wg immunostaining
720 in an undamaged disc (C) and an R24 disc (D-D”). (E-F”) Nub and Wg immunostaining
721 in an undamaged disc (E) and an R24 disc (F-F”). (G-H’) Zfh2 and Wg immunostaining
722 in an undamaged disc (G) and an R24 disc (H-H”). (I-J”) *STAT92E-GFP* expression and
723 Wg staining in an undamaged disc (I) and an R24 disc (J-J”). (K-L”) Zfh2 and Wg
724 staining as well as *nub-GFP* expression in an undamaged disc (K-K’) and an R24 disc
725 (L-L”). Scale bars are 100μm.
726
727

Fig. 5

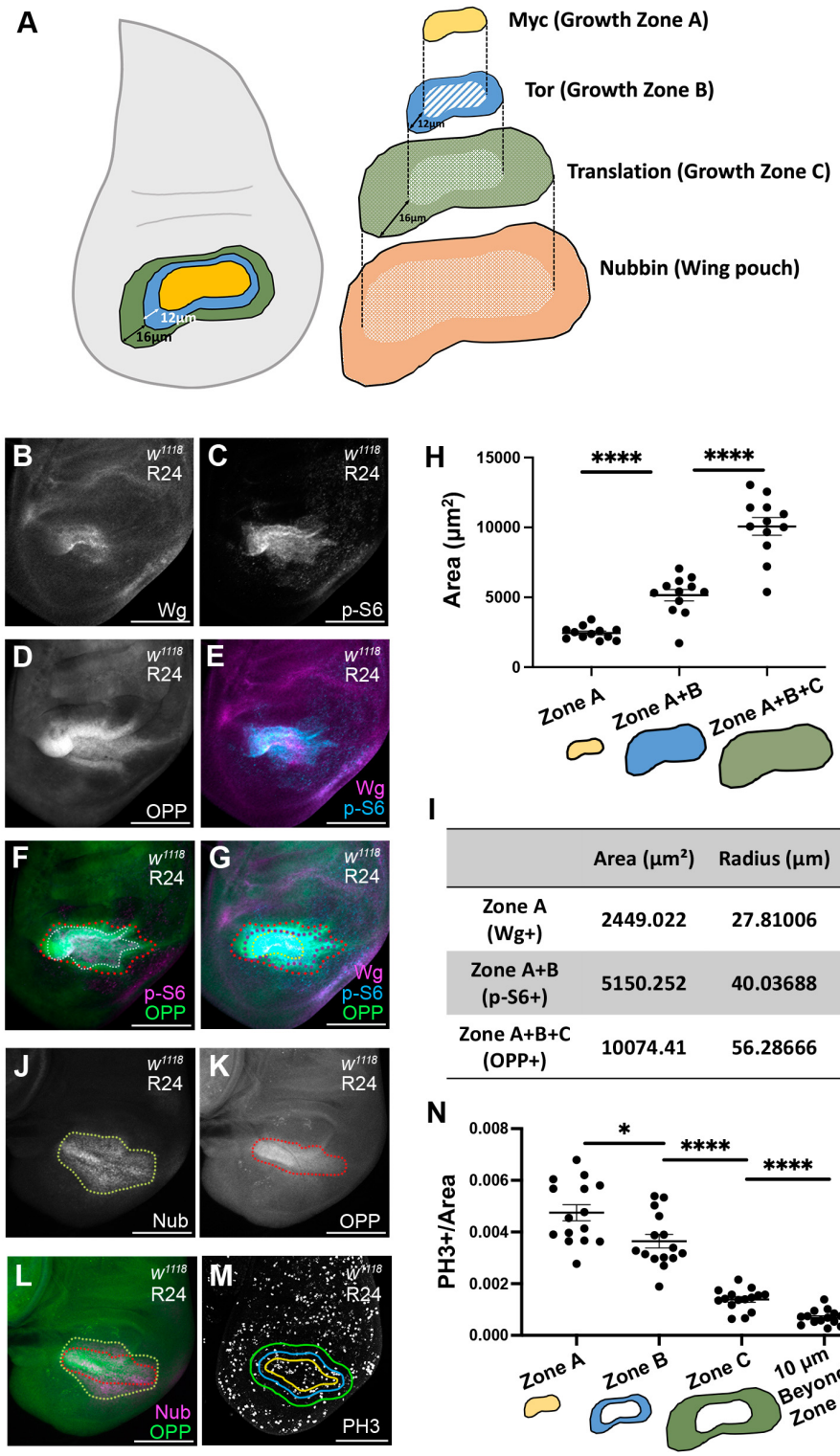

I

	Area (µm²)	Radius (µm)
Zone A (Wg+)	2449.022	27.81006
Zone A+B (p-S6+)	5150.252	40.03688
Zone A+B+C (OPP+)	10074.41	56.28666

728 **Figure 5. Zones of growth in the regeneration blastema**

729 (A) Schematic of concentric growth zones in a regenerating wing disc. (B-G) Wg
730 staining (yellow dashed line), p-S6 staining (white dashed line) and OPP assay (red
731 dashed line) in the same R24 disc. (B) Wg. (C) p-S6. (D) OPP assay. (E) Wg and p-S6.
732 (F) Wg and OPP assay. (G) Wg, p-S6, and OPP assay. (H) Quantification of area in
733 zones identified by Wg, p-S6, and the OPP assay. n=12. ****P<0.0001, Welch's t-test.
734 (I) Average area and radius of each zone. (J-L) R24 disc with Nub staining (J), OPP
735 assay (K), and merged image (L). (M) PH3 staining in an R24 disc. Yellow line outlines
736 Growth Zone A. Blue line outlines Growth Zone B, 13 microns beyond Growth Zone A.
737 Green line outlines Growth Zone C, 16 microns beyond Growth Zone B. (N)
738 Quantification of mitotic cells per area in each growth zone identified as in (M). n=15.
739 *P<0.05, ****P<0.0001, Welch's t-test. Scale bars are 100μm. Error bars are SEM.
740
741

Fig. 6

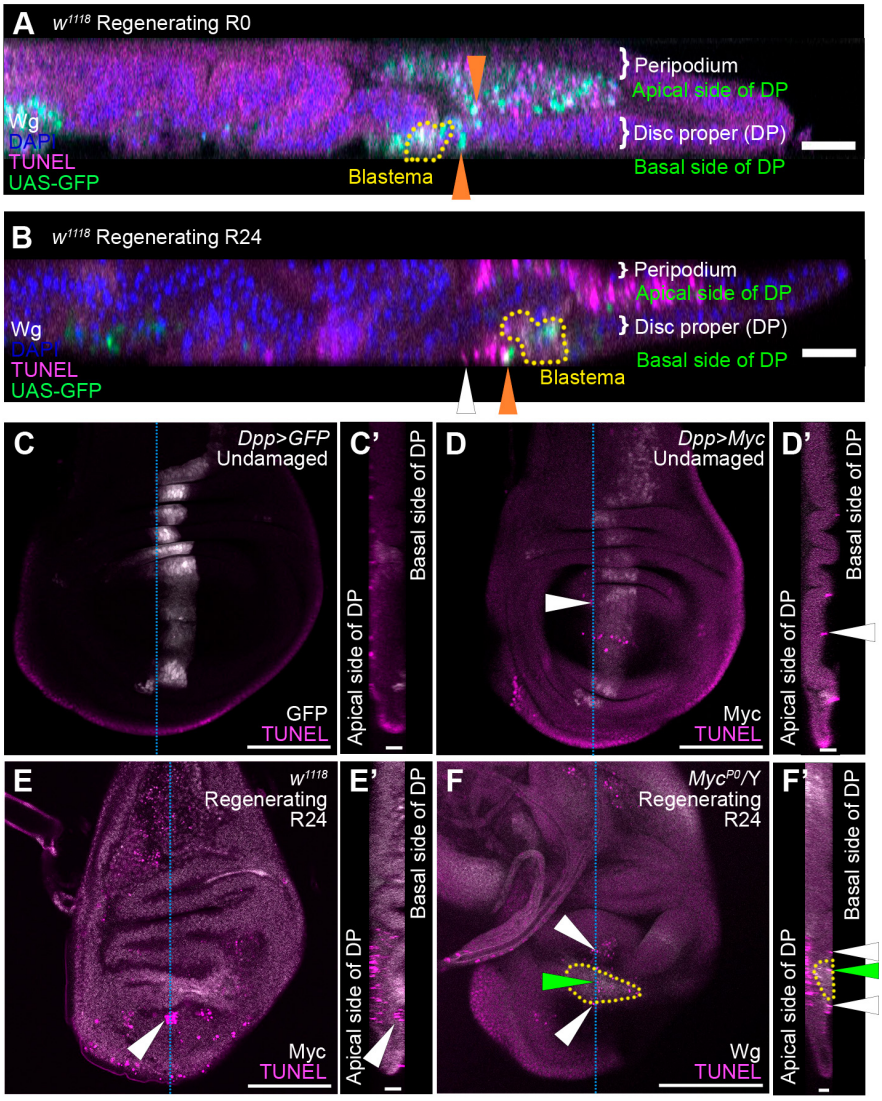
A
w1118 Regenerating R0
Peripodium
Apical side of DP
Disc proper (DP)
Basal side of DP
Wg
DAPI
TUNEL
UAS-GFP
Blastema
B
w1118 Regenerating R24
Peripodium
Apical side of DP
Disc proper (DP)
Basal side of DP
Wg
DAPI
TUNEL
UAS-GFP
Blastema
C
Dpp>GFP
Undamaged
GFP
TUNEL
C'
Apical side of DP
Basal side of DP
D
Dpp>Myc
Undamaged
Myc
TUNEL
D'
Apical side of DP
Basal side of DP
E
w1118
Regenerating
R24
Myc
TUNEL
E'
Apical side of DP
Basal side of DP
F
MycP0/Y
Regenerating
R24
Wg
TUNEL
F'
Apical side of DP
Basal side of DP

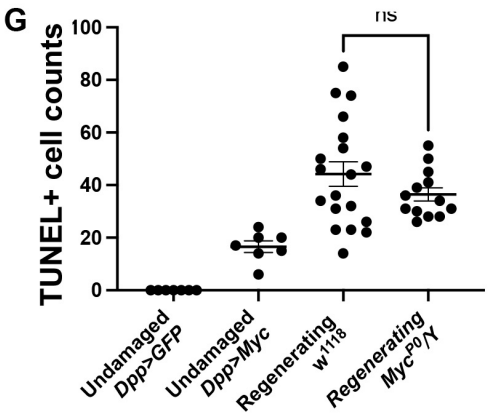
G
TUNEL+ cell counts
100
80
60
40
20
0
ns
Undamaged Dpp>GFP
Undamaged Dpp>Myc
Regenerating w1118
Regenerating MycP0/Y

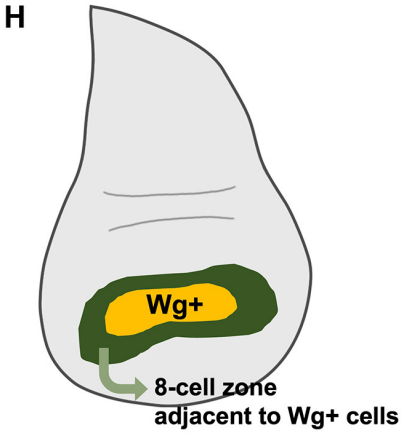
H
Wg+
8-cell zone
adjacent to Wg+ cells

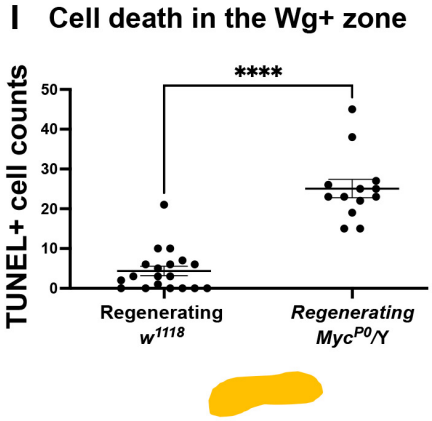
I
Cell death in the Wg+ zone
TUNEL+ cell counts
50
40
30
20
10
0
****
Regenerating w1118
Regenerating MycP0/Y

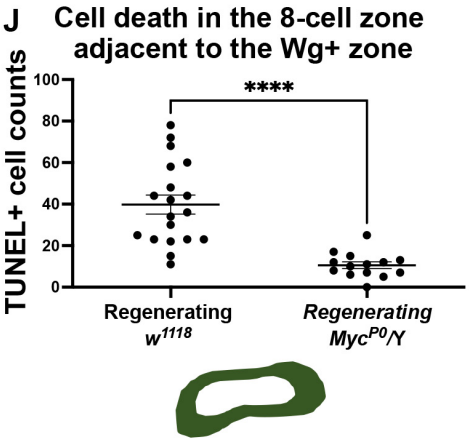
J
Cell death in the 8-cell zone
adjacent to the Wg+ zone
TUNEL+ cell counts
100
80
60
40
20
0
****
Regenerating w1118
Regenerating MycP0/Y

742 **Figure 6. Myc expression induces cell death at the periphery of Growth Zone A**
743 (A-B) Orthogonal views of an R0 disc (A) and an R24 disc (B). Wg staining (white)
744 marks the regeneration blastema (yellow dotted lines). UAS-GFP (green) marks cell
745 debris from tissue ablation. TUNEL assay (magenta) marks debris and apoptotic cells.
746 DAPI (blue) marks nuclei. White arrowhead marks TUNEL+ GFP- apoptotic cell, orange
747 arrowhead marks TUNEL+ GFP+ cell debris. (C-F) TUNEL assay marking apoptotic
748 cells in a negative control (*dpp-Gal4>UASGFP*) (C), positive control
749 (*dppGal4>UASMyc*) (D), w^{1118} R24 disc (E), and Myc^{P0}/Y R24 disc (F). (E) w^{1118} R24
750 disc with Myc staining marking Growth Zone A. (F) Myc^{P0}/Y R24 disc with Wg staining
751 (yellow line) marking Growth Zone A. (C',D',E',F') Orthogonal views of (C,D,E,F). White
752 arrowheads mark apoptosis adjacent to high Myc expression. Green arrowhead marks
753 apoptosis in the blastema. (G) Quantification of cell death labeled by TUNEL at the
754 basal side of the epithelium in the areas that were GFP+ (C) or Myc+ (D) in the wing
755 pouch and an eight-cell band extending anteriorly, or the Wg+ Myc+ blastema and an
756 eight-cell band outside of the blastema. *dpp>GFP* n=7*, dpp>Myc* n=7*,* w^{1118} R24 n=19,
757 Myc^{P0}/Y R24 n=14. n.s. P>0.05, Welch's t-test. (H) Schematic of a regenerating wing
758 disc, yellow indicates the Wg+Myc+ zone, green indicates the eight cells beyond. (I)
759 Quantification of cell death in the Wg+ zone in R24 discs. w^{1118} n=19, Myc^{P0}/Y n=14.
760 ****P<0.0001, Welch's t-test. (J) Quantification of cell death in the eight-cell band
761 outside the Wg+ zone. w^{1118} n=19, Myc^{P0}/Y n=14. ****P<0.0001, Welch's t-test. Scale
762 bars are 100μm. Error bars are SEM.
763
764

Fig. 7

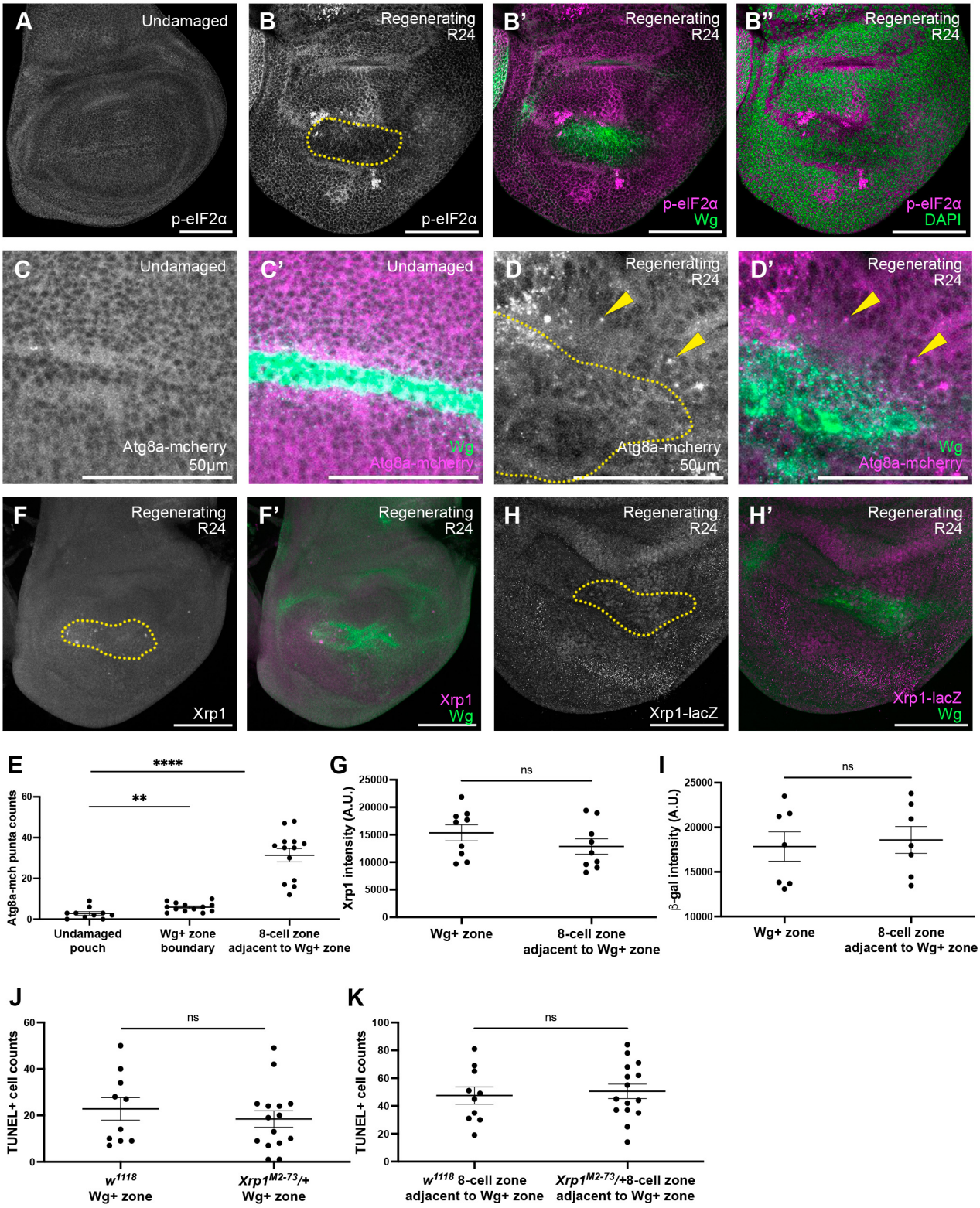
A
Undamaged
p-eIF2α
B
Regenerating R24
p-eIF2α
B'
Regenerating R24
p-eIF2α
Wg
B''
Regenerating R24
p-eIF2α
DAPI
C
Undamaged
Atg8a-mcherry
50μm
C'
Undamaged
Wg
Atg8a-mcherry
D
Regenerating R24
Atg8a-mcherry
50μm
D'
Regenerating R24
Wg
Atg8a-mcherry
F
Regenerating R24
Xrp1
F'
Regenerating R24
Xrp1
Wg
H
Regenerating R24
Xrp1-lacZ
H'
Regenerating R24
Xrp1-lacZ
Wg
E
Atg8a-mch punta counts
****
**
Undamaged pouch
Wg+ zone boundary
8-cell zone adjacent to Wg+ zone
G
Xrp1 intensity (A.U.)
ns
Wg+ zone
8-cell zone adjacent to Wg+ zone
I
β-gal intensity (A.U.)
ns
Wg+ zone
8-cell zone adjacent to Wg+ zone
J
TUNEL+ cell counts
ns
w1118 Wg+ zone
Xrp1M2-73/+ Wg+ zone
K
TUNEL+ cell counts
ns
w1118 8-cell zone adjacent to Wg+ zone
Xrp1M2-73/+8-cell zone adjacent to Wg+ zone

765 **Figure 7. Cell competition induced in regenerating wing discs is distinct from**
766 **experimentally induced cell competition**
767 (A-B) p-eIF2α staining in an undamaged disc (A) and an R24 disc (B). (B') p-eIF2α and
768 Wg. (B") p-eIF2α and DAPI. (C-D) Atg8a-mcherry expression in an undamaged disc (C)
769 and an R24 disc (D). (C'-D') Atg8a-mcherry expression and Wg staining (yellow circle).
770 Arrowheads indicate Atg8a puncta. (E) Quantification of Atg8a puncta. n=13. **P<0.01,
771 ****P<0.0001. (F-F') Xrp1 staining in an R24 disc. Yellow dotted circle indicates
772 blastema marked by Wg. (G) Quantification of Xrp1 intensity. n=9, n.s. P>0.05. (H-H')
773 *Xrp1-lacZ* expression in an R24 disc. Yellow dotted circle indicates blastema marked by
774 Wg. (I) Quantification of average β-gal staining intensity. n=7, n.s. P>0.05. (J-K)
775 Quantification of cell death (TUNEL) in the Wg+ area (J) and in the 8-cell zone adjacent
776 to the Wg+ area (K) in w^{1118} R24 discs and $Xrp1^{M2-73}$/+ R24 discs. w^{1118} n=10, $Xrp1^{M2-}$
777 ^{73}/+ n=15. n.s. P>0.05. Scale bars are 100μm. Error bars are SEM. Statistical test used
778 was Welch's t-test.
779
780

S1

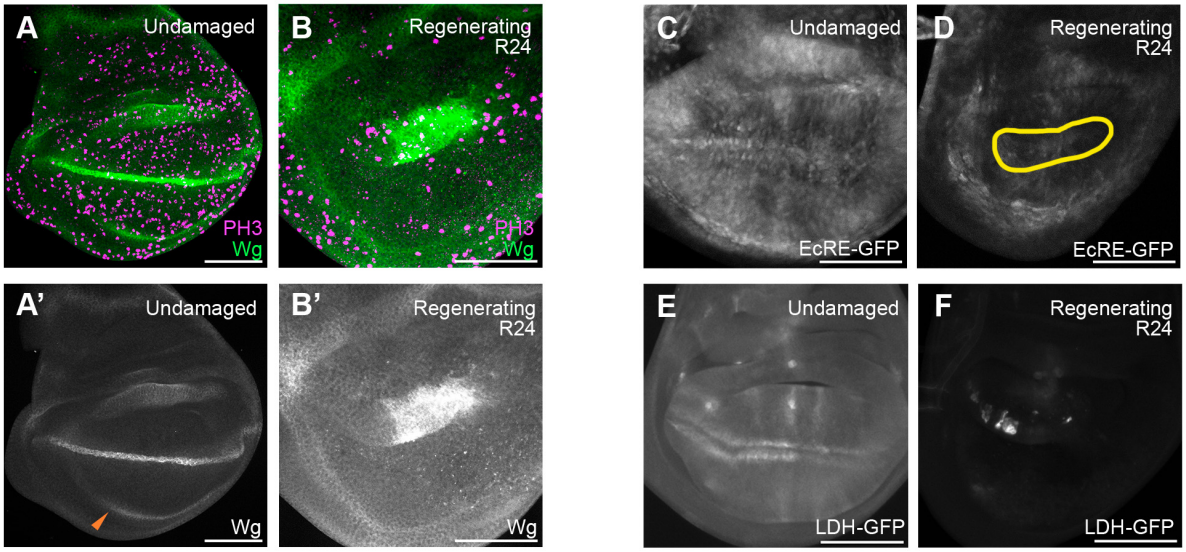
A
Undamaged
PH3
Wg
B
Regenerating
R24
PH3
Wg
C
Undamaged
EcRE-GFP
D
Regenerating
R24
EcRE-GFP
A'
Undamaged
Wg
B'
Regenerating
R24
Wg
E
Undamaged
LDH-GFP
F
Regenerating
R24
LDH-GFP

781 **Figure S1. Ecdysone receptor and Lactate dehydrogenase do not drive**
782 **regenerative growth**
783 (A-B') PH3 staining in an undamaged disc (A-A') and an R24 disc (B-B'). Orange
784 arrowhead in (A') indicates inner ring of Wg. (C-D) EcRE-GFP expression in an
785 undamaged disc (C) and an R24 disc (D). (E-F) LDH-GFP expression in an undamaged
786 disc (E) and an R24 disc (F).
787

S2

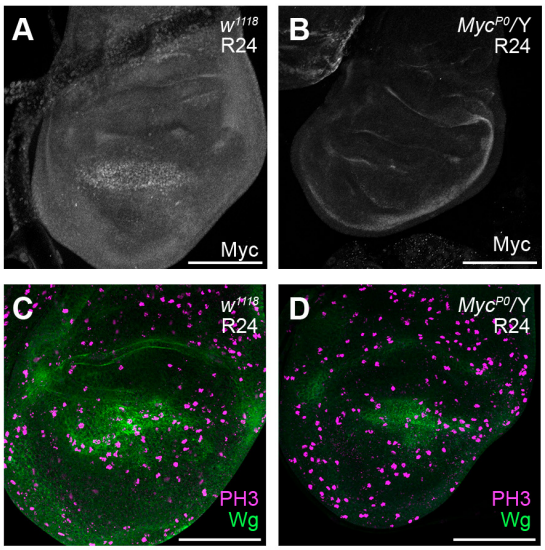
A
w^{1118}
R24
Myc
B
Myc^{P0}/Y
R24
Myc
C
w^{1118}
R24
PH3
Wg
D
Myc^{P0}/Y
R24
PH3
Wg

788 **Figure S2. The *Myc^{P0}* mutation reduces Myc and proliferation during regeneration**

789 (A-B) Myc immunostaining in a *w^{1118}* R24 disc (A) and a *Myc^{P0}/Y* R24 disc (B). (C-D)

790 PH3 staining in a *w^{1118}* R24 disc (C) and a *Myc^{P0}/Y* R24 disc (D).

791

S3

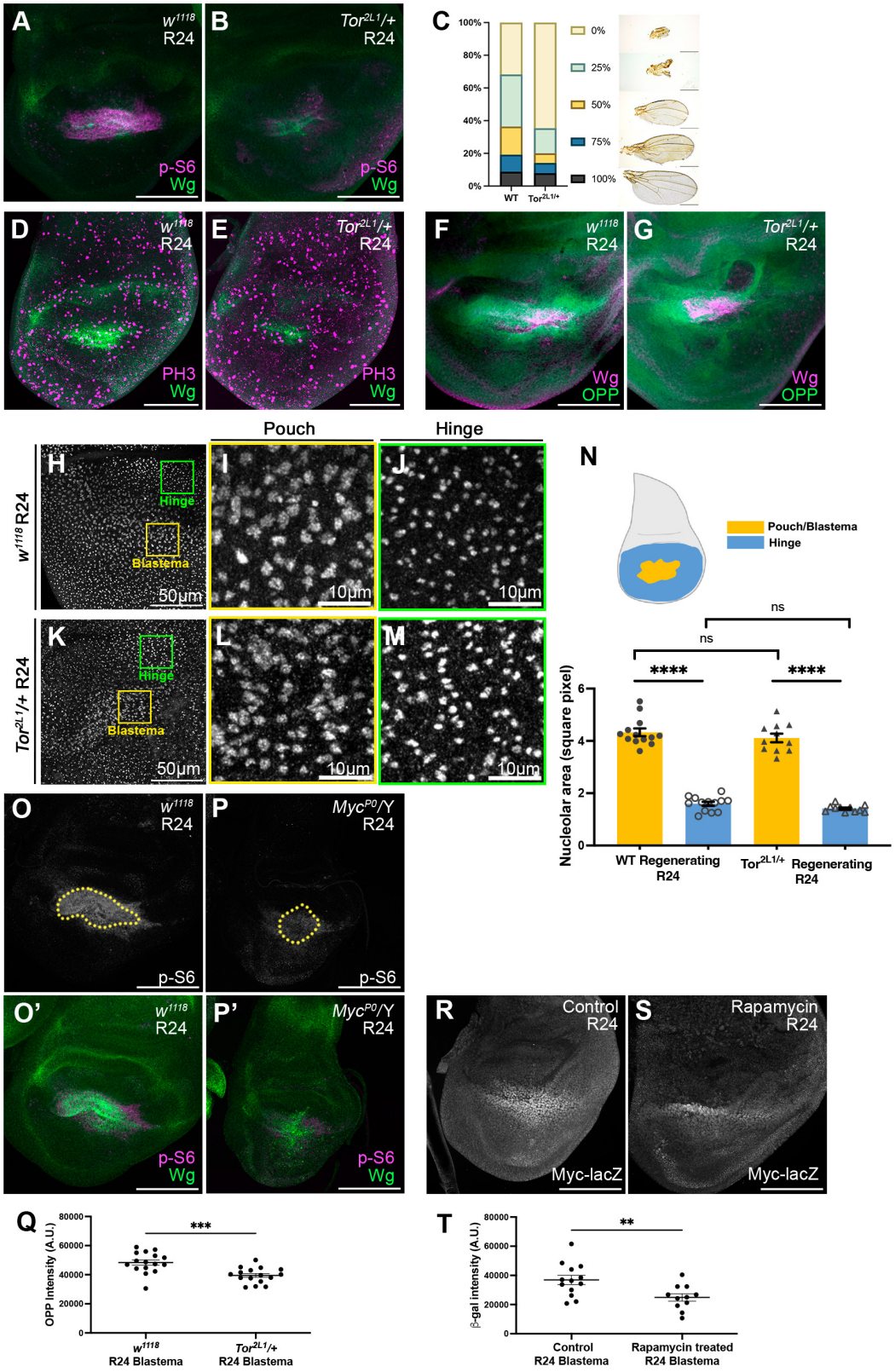
A
w1118
R24
p-S6
Wg
B
Tor2L1/+
R24
p-S6
Wg
C
100%
80%
60%
40%
20%
0%
WT
Tor2L1/+
0%
25%
50%
75%
100%
D
w1118
R24
PH3
Wg
E
Tor2L1/+
R24
PH3
Wg
F
w1118
R24
Wg
OPP
G
Tor2L1/+
R24
Wg
OPP
Pouch
Hinge
H
w1118 R24
Hinge
Blastema
50µm
I
10µm
J
10µm
K
Tor2L1/+ R24
Hinge
Blastema
50µm
L
10µm
M
10µm
N
Pouch/Blastema
Hinge
ns
ns
****
****
Nucleolar area (square pixel)
6
4
2
0
WT Regenerating R24
Tor2L1/+ Regenerating R24
O
w1118
R24
p-S6
P
MycP0/Y
R24
p-S6
O'
w1118
R24
p-S6
Wg
P'
MycP0/Y
R24
p-S6
Wg
R
Control
R24
Myc-lacZ
S
Rapamycin
R24
Myc-lacZ
Q
OPP Intensity (A.U.)
80000
60000
40000
20000
0
***
w1118 R24 Blastema
Tor2L1/+ R24 Blastema
T
β-gal intensity (A.U.)
80000
60000
40000
20000
0
**
Control R24 Blastema
Rapamycin treated R24 Blastema

Figure S3. Effects of the *Tor^{2L1}* mutation on regeneration.

(A-B) p-S6 and Wg staining in a *w^{1118}* R24 disc (A) and a *Tor^{2L1}*/+ R24 disc (B). (C) Size of adult wings after disc regeneration in *w^{1118}* and *Tor^{2L1}*/+ animals. Scale bars are 500μm. (D-E) PH3 staining in a *w^{1118}* R24 disc (D) and a *Tor^{2L1}*/+ R24 disc (E). (F-G) OPP assay with Wg staining in a *w^{1118}* R24 disc (F) and a *Tor^{2L1}*/+ R24 disc (G). (H-M) Fibrillarin staining marking nucleoli in a *w^{1118}* R24 disc (H-J) and a *Tor^{2L1}*/+ R24 disc (K-M). (I, L) 200-pixel^2 area from blastema in H, K accordingly (yellow boxes), identified by Wg staining. (J, M) 200-pixel^2 area from wing hinge in H, K (green boxes). (N) Quantification of nucleolus size in hinge and blastema. Scale bars are 100μm unless otherwise marked. Error bars are SEM. (O-P) p-S6 staining in a *w^{1118}* (O) and a *Myc^{P0}/Y* (P) disc. (O'-P') p-S6 and Wg staining in a *w^{1118}* R24 disc (O') and a *Myc^{P0}/Y* R24 disc (P'). (Q) Quantification of average p-S6 staining intensity in the blastema identified by Wg staining (yellow dotted lines). n=10 *w^{1118}* n=10 , *Myc^{P0}/Y* n=9. **P<0.01. (R-S) *Myc-lacZ* expression marked by β-gal staining in a control R24 disc (R) and a rapamycin-treated R24 disc (S). (T) Quantification of average β-gal staining intensity in the blastema. control n=13, rapamycin n=11. **P<0.01. Statistical test used was Welch's t-test. Scale bars are 100μm unless otherwise marked. Error bars are SEM.

S4

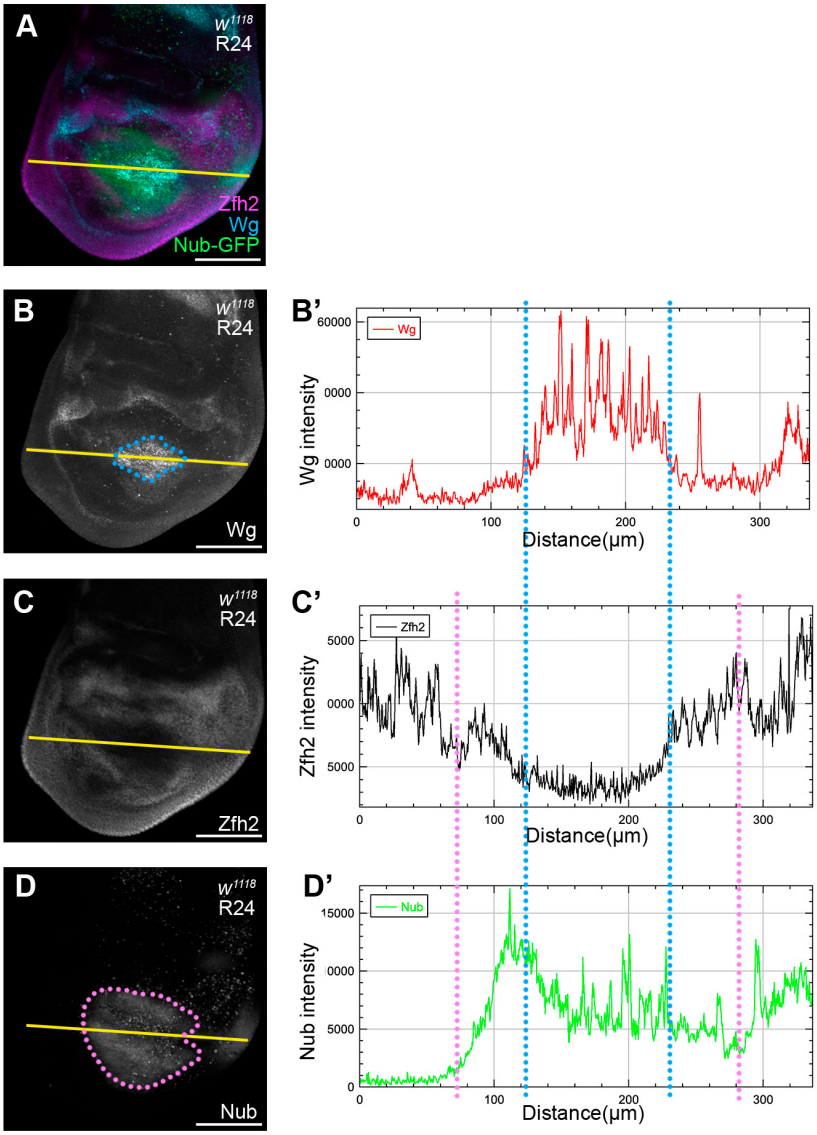
A
w1118
R24
Zfh2
Wg
Nub-GFP
B
w1118
R24
Wg
B'
Wg
Wg intensity
60000
0000
0000
0
100
200
300
Distance(μm)
C
w1118
R24
Zfh2
C'
Zfh2
Zfh2 intensity
5000
0000
5000
0
100
200
300
Distance(μm)
D
w1118
R24
Nub
D'
Nub
Nub intensity
15000
0000
5000
0
0
100
200
300
Distance(μm)

Figure S4. Map of Zfh2, Wg, and Nub expression.

(A) R24 disc expressing *nub-GFP* with Zfh2 and Wg immunostaining. (B) Wg staining. (B') Intensity plot of Wg staining taken from the yellow cross-section line in (B). (C) Zfh2 staining. (C') Intensity plot of Zfh2 staining taken from the yellow cross-section line in (C). (D) *nub-GFP* expression. (D') Intensity plot of GFP taken from the yellow cross-section line in (D). Blue dotted circle in (B) and blue dotted lines in (B'-D') indicate the edge of Wg-expressing area. Pink dotted circle in (D) and pink dotted lines in (C'-D') indicate edge of *nub-GFP* expressing area. Scale bars are 100μm.

S5

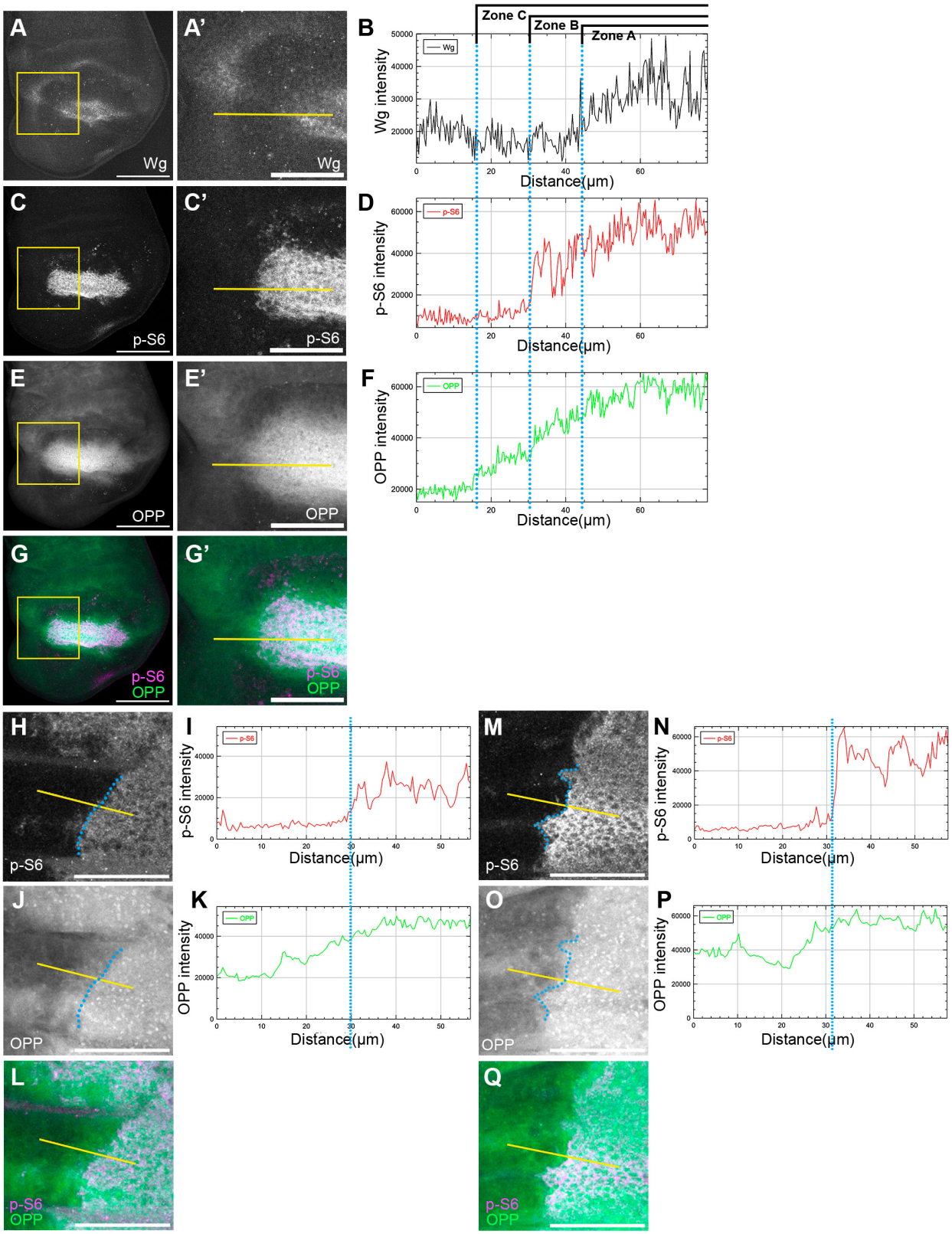
A
A'
Wg
B
Zone C
Zone B
Zone A
Wg intensity
Distance(μm)
C
C'
p-S6
D
p-S6 intensity
E
E'
OPP
F
OPP intensity
G
G'
p-S6
OPP
H
I
J
K
L
M
N
O
P
Q

821 **Figure S5. Map of Wg, p-S6, and OPP in the blastema.**

822 (A,C,E,G) A *w*^{1118} R24 disc with Wg (A) and p-S6 (C) staining, OPP assay (E), and
823 merge of p-S6 and OPP (G). (A',C',E',G') A higher magnification image of the yellow
824 square in (A-G). (B,D,F) Fluorescence intensity plots taken from the yellow line in
825 (A',C',E'). (H-Q) *hhGal4, UAS-Tsc2RNAi* (*hh>Tsc2i*) undamaged discs with p-S6
826 immunostaining (H, M) and OPP assay (J, O). Note (H-K) are from one wing disc and
827 (M-Q) are from another wing disc. (I) Fluorescence intensity plot taken from the yellow
828 line in (H). (K) Fluorescence intensity plot taken from the yellow line in (J). (N)
829 Fluorescence intensity plot taken from the yellow line in (M). (O) Fluorescence intensity
830 plot taken from the yellow line in (P). Blue dotted lines in (H-K) and (M-P) indicate the
831 edge between high/low p-S6 staining. Scale bars are 100μm.

832

833

S6

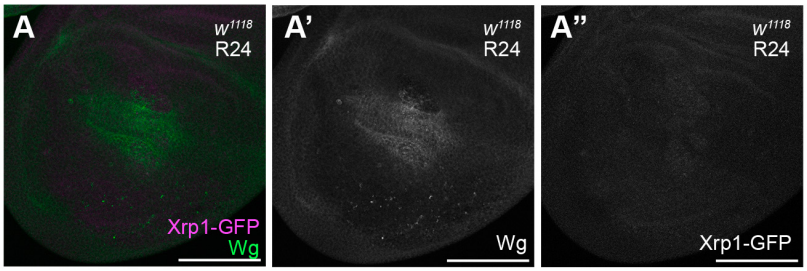

834 **Figure S6. Expression of Xrp1-GFP.**

835 (A-A”) Xrp1-GFP expression in wing disc with Wg staining. (A) merge, (A’) Wg, (A’’)

836 GFP. Scale bars are 100μm.

837